ORNL/TM-2021/2198

Organic Iodide Sorption from Dilute Gas Streams

Allison T. Greaney
Stephanie H. Bruffey
Amy K. Welty *(INL)*
Nick R. Soelberg *(INL)*

September 2021

OAK RIDGE National Laboratory

ORNL IS MANAGED BY UT-BATTELLE LLC FOR THE US DEPARTMENT OF ENERGY

ORNL/TM-2021/2198

Nuclear Energy and Fuel Cycle Division

ORGANIC IODIDE SORPTION FROM DILUTE GAS STREAMS

Allison T. Greaney
Stephanie H. Bruffey
Amy K. Welty (INL)
Nick R. Soelberg (INL)

September 2021

Prepared by
OAK RIDGE NATIONAL LABORATORY
Oak Ridge, TN 37831-6283
managed by
UT-BATTELLE LLC
for the
US DEPARTMENT OF ENERGY
under contract DE-AC05-00OR22725

This page is intentionally left blank.

CONTENTS

ABSTRACT

Reprocessing used nuclear fuel releases volatile radionuclides, including ^{129}iodine (I), into the off-gas of a processing plant. Volatile radioiodine could be present in several forms, depending on the chemistry of the process used and the off-gas stream. Inorganic I_2 is expected to be the predominant I species in the dissolver off-gas (DOG), with minor organic iodides present. The bulk of the I is expected to volatilize into the DOG in parts-per-million-level (ppm) concentrations. In contrast, in the vessel off-gas (VOG), most of the volatile I is expected to be found as organic iodides, such as CH_3I, C_4H_9I, and $C_{12}H_{25}I$. These species are expected to be present in parts-per-billion-level (ppb) concentrations but require abatement, even at low expected concentrations, to meet regulatory emissions limits in the United States. Historically, studies of I abatement by Ag-functionalized sorbents have focused on inorganic I in the DOG, but in the last few years, more research attention has been given to organic iodides, especially longer chain species, such as C_4H_9I, and $C_{12}H_{25}I$.

This report has three main goals: (1) to present new data generated at Oak Ridge National Laboratory (ORNL) in FY21 on the sorption behavior of organic iodides on AgZ, (2) to summarize and synthesize organic iodide data produced by ORNL and Idaho National Laboratory (INL) over the last 4 years to answer questions on organic iodides behavior outlined in the 2018 joint test plan (Jubin et al. 2018), and (3) to propose a VOG abatement system design that can provide the capture efficiencies required to meet I emission limits.

The 2021 ORNL experimental campaign tested the effects of organic iodide speciation and concentration in the off-gas, superficial velocity of the off-gas, and effects of aging on AgZ sorbent capacity. These studies found that the sorption rate of organic iodides by AgZ depends on the hydrocarbon chain length and the concentration in the off-gas. Higher molecular weight organic iodides adsorb to AgZ more slowly than I. At a concentration of 50 ppm concentration in the off-gas, CH_3I loads 8% slower, C_4H_9I loads 20% slower, and $C_{12}H_{25}I$ loads 40% slower than I. The lowest concentration loading rates calculated were in 5 ppm organic iodide gas streams in which AgZ gained on average 0.14 mg I/g sorbent/hour in the bench-scale test system. Thus, longer sorbent beds might be needed to accommodate slower loading rates onto AgZ in lower concentration gas streams. Although sorption rate varies as a function of hydrocarbon chain length, the saturation concentration of the sorbent for these I-bearing species does not vary. Aging AgZ in a humid air stream for 9 months drops the overall sorbent capacity by ~35% for CH_3I, ~50% for C_4H_9I, and ~40% for $C_{12}H_{25}I$. This results in a saturation capacity between 35 and 70 mg I/g sorbent for the aged AgZ.

In conjunction with recent data produced by INL, these data are used to estimate the mass transfer zone (MTZ) and decontamination factor (DF) for sorbent beds of AgZ. Sorption tests performed with iodide gas concentrations of about 1 ppm and higher at a superficial gas velocity of 10 m/min, indicate that MTZ depths for these conditions tend to range between about 8-20 cm. Tests performed at lower concentrations between 50-90 ppb and at gas superficial velocities of 1, 10, and 20 m/min indicate that the MTZ depth increases with increasing superficial gas velocity. The 20 m/min test indicates that the MTZ for those conditions was at least 22 cm, and doubling the superficial gas velocity from 10 to 20 m/min could roughly double or triple the MTZ depth. Doubling and tripling the bounding MTZ depth of 20 cm for the body of MTZ estimates made at with 10 m/min superficial velocity would extend the MTZ for a superficial velocity of 20 m/min to 40-60 cm. This bounding limit applies to all of the organic iodides that have been tested. These results also indicate that the sorption rate-limiting step is not sensitive to the superficial gas velocity; otherwise the MTZ depth would not have increased approximately in proportion to the increase in the gas superficial velocity. This further suggests that the rate limiting step is not associated with mass transfer of the sorbate to the sorbent surface, or mass

transfer of the reaction byproducts from the sorbent surface, but is associated with sorption or chemical reactions on the sorbent surface or in sorbent pores.

Deep bed testing at INL has established DFs of >2,000 for I, CH_3I, and C_4H_9I under a range of conditions (Soelberg et al. 2021, Bruffey et al. 2019). DF does not seem to be affected by the concentration of the organic iodide in the gas stream over the range of 1 to 50 ppm. Thus, if the MTZ is accommodated in sorbent bed design for the DOG and VOG, then regulatory DFs will be met.

To meet the third objective outlined in this report, these experimental data were used to update an engineering evaluation of the VOG first completed in 2016. The updated VOG design can be found in an accompanying document (Welty et al., 2021; INL- LTD-21-64587). This report finds that the VOG will decrease in both size and complexity, relative to previous designs, and will still meet regulatory requirements for all iodine forms.

FIGURES

TABLES

ABBREVIATIONS

AgAero	Ag-functionalized aerogel
BSE	backscattered electron
DF	decontamination factor
DOG	dissolver off-gas
DOE	US Department of Energy
EDS	energy dispersive x-ray spectroscopy
EPA	US Environmental Protection Agency
FID	flame ionization detector
GC	gas chromatography
GC-MS	gas chromatography mass spectrometry
ID	inner diameter
INL	Idaho National Laboratory
LOD	limit of detection
LOQ	limit of quantification
MS	mass spectrometry
MTZ	mass transfer zone
NAA	neutron activation analysis
NE	Office of Nuclear Energy
NRC	US Nuclear Regulatory Commission
ORNL	Oak Ridge National Laboratory
PNNL	Pacific Northwest National Laboratory
SE	secondary electron
SEM	scanning electron microscopy
SPME	solid phase micro extraction
TBP	tri-*n*-butyl phosphate
TGA	thermogravimetric analyzer
VOG	vessel off-gas

1. INTRODUCTION

In the 1960s, multiple researchers unexpectedly observed that there appeared to be a type of iodine-bearing species bypassing the sorbents that were then most commonly used for the abatement of gaseous radioactive I (Adams et al. 1967, Billard 1967, Parker 1964, Browning 1963). These observations were first made in the context of potential I releases from severe nuclear reactor accidents and spawned multiple studies to better understand the behavior of I within trapping or sorption systems. After some investigation, the consensus was that the form of I penetrating through the sorbent systems was CH_3I, a highly volatile organic I-bearing species (Browning 1963). The potential existence of a second penetrating I form, thought to be inorganic HOI or HI, was noted in the 1970s (Dexter 1977; Jubin 1981), but this has not been confirmed to date.

From the late 1970s to the early 2000s, relatively limited information on CH_3I sorption was published. These studies focused on CH_3I removal by different materials, including common adsorbents, such as Ag faujasite and 13× molecular sieves, as well as $AgNO_3$ mounted or impregnated onto nonreactive supports (Pence et al. 1972, 1973; Ackley and Combs 1973; Jubin 1981; Broothaerts 1976; Wilhelm and Schuttelkopf 1970; Evans and Jervis 1992). Some of these materials were shown to have the ability to sorb CH_3I, and their capacities and sorption rates were characterized for a narrow envelope of experimental conditions. Although the published data are informative for sorbent selection and in providing a preliminary understanding of factors that affect CH_3I sorption by the tested materials, it was insufficient for understanding how CH_3I removal could be achieved in an operating facility.

The 2009 formation of a multi-laboratory collaboration within the United States sponsored by the US Department of Energy's (DOE's) Office of Nuclear Energy (NE) reinvigorated interest in the topic of volatile I management within nuclear fuel reprocessing facilities. The Off-Gas Sigma Team was formed to decrease or remove technological barriers that could complicate or prevent the reduction of radioactive emissions from nuclear fuel reprocessing facilities. One of the first significant analyses performed under this collaborative framework was an examination of US regulations that could be applicable to the gaseous radioactive emissions from an aqueous-based nuclear fuel reprocessing facility (Jubin et al. 2012). Key volatile radioactive emissions from an aqueous-based nuclear fuel reprocessing facility include ^{3}H as $^{3}H_2O$, ^{14}C as $^{14}CO_2$, ^{85}Kr, and ^{129}I as multiple chemical species.

This analysis found that three key regulations could limit the emissions of volatile radionuclides from a nuclear fuel reprocessing plant: (1) US Environmental Protection Agency (EPA) environmental standards for the U fuel cycle in 40 CFR 190.10 (EPA 2010a), (2) EPA national standards for hazardous air pollutants in 40 CFR 61 (EPA 2010b), and (3) US Nuclear Regulatory Commission (NRC) standards for protection against radiation in 10 CFR 20 (NRC 2012). 40 CFR 190.10(a) explicitly limits the annual whole-body dose and the annual thyroid dose that may be received by a member of the public as a result of U fuel cycle operations. Nearly the entire thyroid dose would result from ^{129}I absorption. 40 CFR 190.10(b) limits the total amount of ^{129}I that can be released during the U fuel cycle:

> §190.10(a): The annual dose equivalent does not exceed 25 millirems to the whole body, 75 millirems to the thyroid, and 25 millirems to any other organ of any member of the public as the result of exposures to planned discharges of radioactive materials, radon and its daughters excepted, to the general environment from uranium fuel cycle operations and to radiation from these operations…

and

> §190.10(b): The total quantity of radioactive materials entering the general environment from the entire uranium fuel cycle, per gigawatt-y of electrical energy produced by the fuel cycle, contains less than 50,000 curies of krypton-85, 5 millicuries of I-129, and 0.5 millicuries combined of plutonium-239 and other alpha-emitting transuranic radionuclides with half-lives greater than one year.

Jubin et al. (2012) found that applying the limits in 40 CFR 190.10 to an aqueous-based commercial nuclear fuel reprocessing facility in the United States would, in the most conservative case, result in required decontamination factors (DFs) for radioactive ^{129}I of 8,000, and less conservative scenarios would still require a minimum ^{129}I DF of 1,000. The DF is the ratio of the uncontrolled emission rate of a radionuclide to the highest emission rate that would meet the assumed regulatory limits. A DF of 1,000 corresponds to an I removal efficiency of 99.9%, and a DF of 8,000 corresponds to an I removal efficiency of 99.9875%.

This study was pivotal in demonstrating the magnitude of the I treatment problem that would be faced by aqueous-based nuclear fuel reprocessing facilities within the United States. Although I removal technologies exist, demonstrating that these technologies can achieve these removal efficiencies across a complex aqueous reprocessing facility had never been attempted. Furthermore, the size, complexity, and cost of a such an I removal system in an operational facility was likely to be substantial. For these reasons, a comprehensive I emissions control R&D program were initiated by the Off-Gas Sigma Team to provide solutions to this challenge.

1.1 IODINE DISTRIBUTION WITH AN AQUEOUS-BASED NUCLEAR FUEL REPROCESSING FACILITY

To understand the R&D program initiated by the Off-Gas Sigma Team, the work accomplished to-date by the team and other researchers in the field, and the motivation for the experimental testing described in this report, it is important to first understand expected iodine behavior within an aqueous-based nuclear fuel reprocessing facility.

Iodine is produced in nuclear fuel through the spontaneous fission of uranium. Irradiated uranium oxide fuel with a burn-up of 60 GWd/tIHM will contain approximately 291 g of ^{129}I/tIHM (Jubin et al. 2012). This I is contained primarily within the fuel matrix, although some can migrate into the interpellet or plenum spaces of a fuel rod. In the industrialized implementation of aqueous-based nuclear fuel reprocessing, cooled irradiated fuel bundles are sheared to produce ~1 in. long fuel rod segments. These segments are transferred to a dissolution step in which the fuel matrix is dissolved by heated nitric acid. After dissolution, the U—and Pu and other transuranic elements, depending on the chosen separations process—contained within the dissolved fuel is separated and purified by liquid-liquid solvent extraction. The raffinate that contains waste fission products is then converted to stable storage or disposition forms.

As summarized in Jubin et al. (2013), I is released into plant off-gases during each of these steps. These plant off-gases serve multiple purposes, such as to sparge the dissolver solution or vent the liquid-liquid extraction vessel, and each process gas stream will contain I volatilized from these fuel processing operations. It is estimated that 0.5% of the I inventory will be released during shearing, 95% of the I inventory will be released during dissolution, and 2% of the I inventory will be released during liquid-liquid extraction. The balance of the I inventory will be released during waste processing. A visual representation of this is shown in Figure 1.

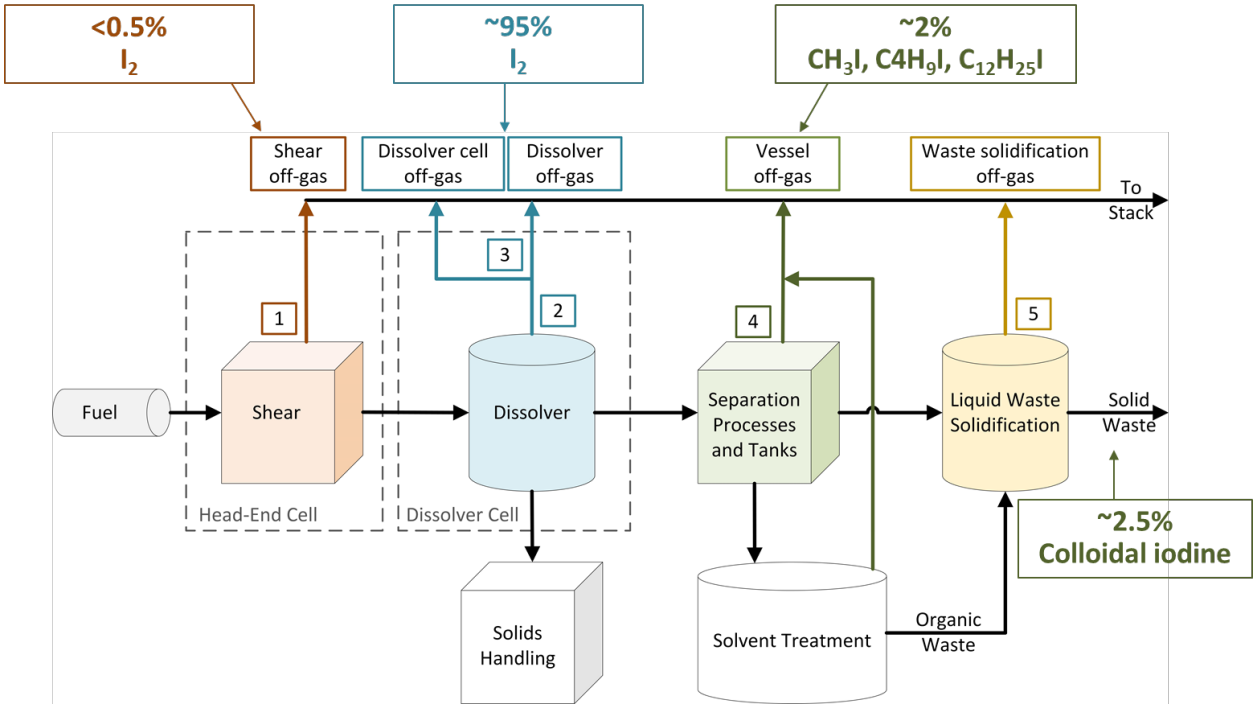

Figure 1. **I volatilization within an aqueous-based nuclear fuel reprocessing facility.** Adapted from Jubin et al. (2013).

Figure 1 illustrates three key aspects of I management within an aqueous-based nuclear fuel reprocessing facility: (1) that I is released into multiple process streams; (2) that the expected release fractions for each individual stream are all less than 99.9%, indicating that multiple streams must be treated to achieve an I DF of 1,000; and (3) that two primary forms of I that are expected to be released: inorganic I_2 and complex organic iodides (CH_3I, C_4H_9I, and $C_{12}H_{25}I$). This figure clearly demonstrates that **effective regulation-compliant I management within an aqueous-based nuclear fuel reprocessing plant must be able to sequester both inorganic and organic forms of I from multiple off-gas streams.**

1.2 CHARACTERISTICS OF DISSOLVER OFF-GAS AND VESSEL OFF-GAS

The two most significant I release points are that of the dissolver off-gas (DOG) and the liquid-liquid extraction vessel off-gas (VOG). These off-gas streams arise from different unit operations and have markedly different characteristics. The expected composition of the DOG and the VOG are summarized in **Table 1**.

Table 1: **Characteristics of the DOG and VOG streams**

Characteristic	DOG	VOG
I concentration	Parts-per-million levels	Parts-per-billion levels
Relative fraction of plant iodine	95%	2%
I speciation	Predominantly inorganic	Predominantly organic
Humidity	10–40°C dew point	0–10°C dew point
NOx concentration	1–2 vol %	< 0.1 vol %
Flow rate	~ 10 LPM	~100 LPM

A substantial body of work can be applied to the design of DOG I abatement systems. Compared with the removal of organic iodine, the removal of inorganic iodine was historically more fully investigated. The primary technical difficulties related to I removal from the DOG are sorbent degradation or capacity loss due to sorbent corrosion, which is sometimes referred to as *sorbent aging*, and the high level of solid sorbent consumption that occurs if preliminary bulk aqueous I scrubbing is not employed (Jubin et al. 2018).

Understanding the removal of I from the VOG presents very different challenges than those of the DOG. First, the parts-per-billion levels of I present in the stream can make all aspects of experimentation challenging. Real-time weight measurements, which can inform sorption rate testing, require a high degree of precision because the sorbent material might only absorb submilligram amounts of I per hour. Measurements of inlet and effluent gas concentrations can also be challenging, requiring extended sampling or other methods with parts-per-billion or parts-per-trillion detection limits. Generating very low-concentration I-bearing streams can require multiple dilution stages, and recovering all volatilized material to complete mass balance is daunting given the very small mass of material that is volatilized per test.

Second, the predominance of organic iodides within the VOG means that there are limited published data that could inform a VOG I abatement system design. As stated previously, CH_3I sorption data could be used in sorbent selection, but these data were insufficient for understanding how CH_3I removal could be achieved in an operating facility. Furthermore, published data were limited to CH_3I, and no other organic iodides had been studied in the context of off-gas treatment for a nuclear fuel reprocessing facility until the initiation of the Off-Gas Sigma Team R&D program. Because VOG is expected to contain multiple organic I species (Bruffey et al. 2015), a full understanding of the removal of multiple organic iodide species is required to meet the stringent emissions requirements dictated by US regulations.

Third, performing I sorption tests with such low I gas concentrations requires a long test duration, often exceeding 1,000 test hours and many months.

1.3 RECENT R&D EFFORTS FOCUSED ON ORGANIC IODIDE ABATEMENT

The most significant body of work related to the topic of organic iodide sorption from dilute gas streams is that performed by Idaho National Laboratory (INL) and Oak Ridge National Laboratory (ORNL) under the auspices of the Off-Gas Sigma Team and DOE NE.

The first report issued under this framework was that of Haefner and Soelberg (2009), which observed that CH_3I may be catalyzed to I_2 across an Ag-sorbent bed. In 2013, a multi-laboratory test plan was designed to continue to investigate fundamental scientific questions about CH_3I sorption by Ag sorbents (Jubin et al. 2013). From this work, a proposed catalytic absorption pathway was proposed by Chapman et al. (2011). Around this time, INL initiated a program of deep-bed sorption testing with CH_3I as the sorbate. These tests were of extended duration (often months) and determined the DFs that could be achieved across different test conditions. CH_3I concentrations in these tests were typically orders of magnitude higher than those that could be expected in the VOG (Soelberg and Watson 2014, 2015).

In 2017, ORNL performed an extensive testing program aimed at understanding CH_3I sorption at concentration levels that could reflect the VOG (Jubin et al. 2017). This work built on several preliminary tests conducted in 2015 and 2016 and attempted to assess how CH_3I concentration could impact sorbed I distribution within a deep test bed (Bruffey et al. 2016). Results indicated that CH_3I was likely to penetrate further into sorbent beds than would I_2.

Coincident with these experimental efforts, a preliminary engineering design for radioactive off-gas treatment systems was produced by ORNL, INL, and Pacific Northwest National Laboratory (PNNL) (Jubin et al. 2016). This design produced initial estimates of mass balances, bed sizing, and bed changeout requirements for the DOG and VOG I removal systems. The VOG design was especially challenging because of the limited information available on organic iodide sorption for relevant conditions and the relatively large gas flowrates that could dictate large cross sections or multiple parallel sorbent beds. Design assumptions included a significant amount of conservatism to compensate for the lack of reliable data, and the resulting system design was large, requiring up to fifteen 0.97 m diameter sorbent cartridges.

In 2018, ORNL and INL developed a joint test plan designed to identify remaining knowledge gaps surrounding organic iodide sorption from dilute gas streams and answer them through a collaborative test program (Jubin et al. 2018). This test plan addressed some fundamental I sorption questions but also sought to provide more applied data that could be useful in the redesign of a VOG I abatement system. ORNL and INL have executed this test plan. Preliminary results were documented in Bruffey et al. (2019) and Soelberg et al. (2021). Testing at INL was completed in April 2021 and testing at ORNL was completed in August 2021.

While the Off-Gas Sigma Team completed its work, two other programs initiated significant experimental efforts related to organic iodide sorption. The first program was a collaboration between Syracuse University and the Georgia Institute of Technology. These universities aligned their research to support the efforts of ORNL and INL and were awarded a Nuclear Energy University Partnership grant from DOE to study organic iodide sorption from dilute gas streams. Their work has experimental and computational aspects and has examined the sorption of CH_3I and $C_6H_{13}I$ at dilute concentrations (Tavlarides et al. 2015). The second program was a multi-laboratory collaboration in France. This effort has focused on CH_3I sorption by zeolite minerals. Publications have been issued that describe analytical examinations of zeolite-sorbed CH_3I, the effects of temperature and moisture on methyl I sorption by zeolite minerals, and the stability of AgI precipitates on zeolite minerals (Chebbi et al. 2016, Nenoff et al. 2014).

1.4 ORGANIC IODIDE SELECTION FOR EXPERIMENTAL WORK

Three organic iodides were selected for off-gas studies at INL and ORNL in 2018: CH_3I, C_4H_9I, and $C_{12}H_{25}I$ (Jubin et al. 2018). These organic iodides are hypothesized to form in the off-gas due to reactions with the organic solvent and diluent used in a typical PUREX reprocessing scheme. Tri-*n*-butyl phosphate (TBP) is used as the main organic extractant, and reactions between TBP and I in solution are hypothesized to produce iodobutane: C_4H_9I. Dodecane or kerosene are used as diluents, and reactions with I in the diluent could form iodododecane: $C_{12}H_{25}I$. Radiolytic degradation of these solvents and diluents might form a range of alkanes that could react to form other I species, including CH_3I (Jubin et al. 2018). The vapor pressures of these three organic iodides varies with hydrocarbon chain length, with CH_3I being the most volatile organic iodide and $C_{12}H_{25}I$ being the least volatile (Table 3). Thus, at the range of operating temperatures in a reprocessing facility, CH_3I and C_4H_9I are the most likely organic iodides to be present in the off-gas and $C_{12}H_{25}I$ is the least likely organic iodide to be present in the off-gas. Although these iodide species are predominantly expected to reside in the VOG, trace organics present in the aqueous phase used for fuel dissolution could also result in minor organic iodide formation in the dissolver, which would evolve into the DOG.

Possible reactions between organic iodides and silver in an Ag-based sorbent are presented in Table 2. The resulting iodide retained on the sorbent is likely in the form of AgI or $AgIO_3$. The abatement of CH_3I in off-gas streams has been the subject of experiments for the past four decades (e.g., Jubin 1981, Scheele et al. 1983) and the sorption mechanisms of this organic iodide on to AgZ has been characterized (Chebbi et al. 2016, Nenoff et al. 2014). However, there was no publicly available literature on the abatement of

C_4H_9I or $C_{12}H_{25}I$ prior to the Off-Gas Sigma Team studies. This report presents new data for C_4H_9I and $C_{12}H_{25}I$ and synthesizes data collected for all three organic iodides at ORNL and INL in the last few years.

Table 2. Possible reactions that occur between organic iodides and silver and the associated Gibbs Free Energy, calculated at 200°C. The formation of AgI and butanol during the reaction between butyl iodide and silver is not thermodynamically favored.

Organic Iodide	Equation	Sorbed iodide	ΔG
			kJ/mol I
CH_3I	$Ag + CH_3I(g) + H_2O(g) = AgI + CH_3OH(g) + 0.5H_2(g)$	AgI	-6.11
CH_3I	$2Ag + 2CH_3I(g) + 3.5O_2(g) + H_2O(g) = 2AgIO_3 + 2CH_3OH(g)$	$AgIO_3$	-93.2
CH_3I	$2Ag + 2CH_3I(g) = 2AgI + C_2H_6(g)$	AgI	-88.1
CH_3I	$2Ag + 2CH_3I(g) + 3O_2(g) = 2AgIO3 + C_2H_6(g)$	$AgIO_3$	-64.9
C_4H_9I	$Ag + C_4H_9I(g) + H_2O(g) = AgI + C_4H_9OH(g) + 0.5H_2(g)$	AgI	30.6
C_4H_9I	$2Ag + 2C_4H_9I(g) + 3.5O_2(g) + H_2O(g) = 2AgIO_3 + 2C_4H_9OH(g)$	$AgIO_3$	-56.5
C_4H_9I	$2Ag + 2C_4H_9I(g) + 5.5O_2(g) = 2AgI + 2C_2H_6(g) + 3H_2O + 4CO_2(g)$	AgI	-1222
C_4H_9I	$2Ag + 2C_4H_9I(g) + 8.5O_2(g) = 2AgIO_3 + 2C_2H_6(g) + 3H_2O + 4CO_2(g)$	$AgIO_3$	-1199

1.5 REPORT AIMS

The sizeable amount of recent experimental work conducted under the auspices of DOE NE successfully addressed many of the technical questions brought forth in Haefner and Soelberg (2010), Jubin et al. (2013), Bruffey et al. (2015), and Jubin et al. (2018). Some of the remaining gaps outlined in the joint test plan (Jubin et al. 2018) were studied at ORNL in FY21 and are not yet published. This report has three main goals.

First is to document the recent work conducted at ORNL in studying the sorption of CH_3I, C_4H_9I, and $C_{12}H_{25}I$ by Ag-based sorbents.

Second is to comprehensively assess the data collected from 2014 to 2021 at ORNL and INL on the topic of organic iodide sorption from dilute gas streams and use these data to present a detailed understanding of how organic iodides might behave within an off-gas treatment process.

Third is to use more realistic assumptions, where possible, to develop an improved VOG treatment design capable of achieving I DFs >1,000.

1.6 JOINT TEST PLAN FOR THE EVALUATION OF IODINE RETENTION FOR LONG-CHAIN ORGANIC IODIDES

The *Joint Test Plan for the Evaluation of Iodine Retention for Long-Chain Organic Iodides* (Jubin et al., 2018) was focused on providing key data about organic iodide sorption that would be important in the development of a VOG iodine removal system. To this end, a series of questions was developed and the tests and systems needed to answer these questions were identified. The key developed questions are as follows.

1. Is iodide sorption rate a function of organic iodide hydrocarbon chain length?

2. Is iodide sorption rate a function of organic iodide concentration in the gas stream?

3. What is the saturation concentration of I for various organic iodides on AgZ, and does it vary with hydrocarbon chain length?

4. Does the ratio of physisorption to chemisorption vary with hydrocarbon chain length?

5. How does gas velocity affect the sorption of organic iodides to AgZ?

6. Do organic iodides follow similar sorption pathways onto AgZ?

7. What is the length and shape of the MTZ, and how do they vary or change for CH_3I and other organic iodides on Ag-based sorbents?

8. What is the DF over a fixed length of bed as a function of concentration and I species in the feed gas?

Many of these questions center around extending the understanding of not just CH_3I sorption but also the understanding of the sorption of other potential I-bearing compounds. Studies indicated that alkyl iodides present in the VOG could include even relatively high molecular weight compounds, such as $C_{12}H_{25}I$. Understanding the variations in sorption rate, sorbent saturation, chemisorption fraction, MTZ, and DF that could occur across this suite of potential compounds was addressed by questions 1, 3, 4, 7, and 8.

Before the development of the joint test plan, no sorption testing that used longer-chain organic iodides had been reported in the context of I removal from nuclear fuel reprocessing off-gas streams. As a result, the data and experience collected during the collaborative effort represent a unique knowledge base internationally. For the purposes of the joint test plan, the decision was made to test CH_3I and $C_{12}H_{25}I$ as bounding members of the alkyl iodide series and to test C_4H_9I as an intermediate point.

Question 2 reflected the uncertainty surrounding a key parameter: that of I concentration in the gas stream. It was unknown whether the findings of parts-per-million-level organic iodide testing would translate to lower gas-phase concentrations. The possibilities that highly dilute streams could be rate-limited by different mechanisms than higher-concentration streams, that extrapolations collected at high parts-per-billion or low parts-per-million concentrations would not reflect dilute gas behavior, and the potential that highly dilute sorbates could bypass a sorbent bed were all concerns that prompted the desire to better understand sorption dependence across a wide range of I concentrations. Results collected at ORNL in 2017 for the CH_3I concentration range of 40 to 1,000 ppb indicated that sorption might not be strongly affected by changing gas-phase sorbate concentrations, but this finding had not yet been confirmed for other organic iodide species.

Question 5 focused on a very practical sorption parameter: gas flow velocity. At the time of writing, the majority of inorganic and organic iodide sorption data had only been collected at relatively low ($\leq$10 m/min) superficial velocities. This flow velocity is more reflective of DOG conditions, and VOG flow velocities are likely to be higher. Reliable engineering designs must have some data on which to base the designs of higher velocity I removal systems. The increased flow velocity might affect the penetration depth of the I into the sorbent bed and/or the total sorbent capacity.

Finally, question 4 asked a very fundamental question regarding whether what was known about CH_3I sorption pathways could be extended to the sorption of other organic iodides. Understanding the similarities between the sorption pathways of multiple species could provide insight into the level of resolution required to effectively understand the behavior of the suite of organic iodide compounds that could be present within the VOG. As mentioned previously, a recent ORNL report provided preliminary

results to this question and found that the sorption pathway for CH_3I might not be directly translated to the sorption of C_4H_9I (Greaney and Bruffey 2021).

2. METHODS AND MATERIALS

Experimental testing at ORNL used both thin and deep beds of sorbent material to assess sorption parameters. Thin-bed tests were performed in a custom-built thermogravimetric analyzer (TGA) capable of continuous sorbent weight measurements and were used to determine the sorption rate and sorbent saturation point. Deep-bed testing was performed for experiments that use very low I concentrations and provided an understanding of how I would distribute through sorbent columns. In some cases, effluent species were monitored by gas chromatography (GC) mass spectrometry (MS) (GC-MS). The test systems, materials, and methods used are described here. A complete description of all systems, materials, and methods used for all testing referenced in this report would be redundant with previous reporting, so only general descriptions are provided for reference with detailed information added for ORNL testing not previously reported. Additionally, a short description of the test systems at INL is included so that comparisons between ORNL and INL data can be understood. Due to differences in how each lab reports data, reported length measurements are given in both inches and centimeters.

2.1 SORBENTS

ORNL and INL testing primarily focuses on two Ag-based sorbents: AgZ and Ag-functionalized aerogel (AgAero). Ag-based sorbents are leading candidate materials for I removal largely because of the irreversible chemisorption of I by Ag and the formation of insoluble, low-vapor pressure, highly stable AgI. Reduced AgZ is a well-characterized I sorbent that has been used in I-capture tests for decades (e.g., Scheele et al. 1983). AgAero is a newer sorbent developed by PNNL that is still undergoing optimization (Matyas et al. 2018, 2019, 2020). This report focuses on the sorption of I by AgZ, but will reference AgAero results as merited.

2.1.1 Silver Mordenite

AgZ was procured from Molecular Products (Ionex-Type Ag sorbent) with a ~0.16 cm pellet diameter and ~0.3 cm length. Different batches of Ionex AgZ contain between 9.5 wt % and 11 wt % Ag. The I capacity of the sorbent, which is as low as 25 mg I/g AgZ upon receipt, is optimized by chemically reducing any oxidized Ag before testing. This reduction can increase the I capacity of AgZ to the theoretical maximum (100% Ag utilization).

Chemical reduction of the Ag is performed by exposing AgZ to a flowing Ar stream for at least 1 day followed by a 4% H_2 blend in N for 10 days. The sorbent material is held at 270°C throughout the reduction, and the gases are preheated before sorbent contact. After reduction, the AgZ is stored under an Ar blanket to limit oxidation by air. The system used for reduction can produce 250 g batches. Each batch of reduced AgZ is exposed to I_2-bearing gas streams via ORNL's thin-bed TGA test system and typical test conditions. This establishes the baseline capacity for each batch, which typically ranges from 80 to 120 mg I/ g sorbent under typical thin-bed testing conditions. I capacity can vary based on the Ag content of the sorbent, reduction time, and sorbent aging that can occur during I sorption.

2.1.2 Silver-Functionalized Silica Aerogel

The development of AgAero underwent multiple iterations over the last few years (Matyas et al. 2018, 2019, 2020) with the goal of optimizing I capacity and sorbent stability in varying off-gas conditions.

Given the evolving nature of this sorbent, the loading rate and maximum loading capacities of different batches of AgAero might differ substantially, and absolute value comparisons are not possible.

AgAero was provided by PNNL with typically one to two batches of material provided per year. Like AgZ, AgAero also undergoes a Ag reduction, which is performed at PNNL before shipment. The AgAero varies from ~1 to ~5 mm-sized particles, depending on the batch. I loading capacity also varies, depending on the sorbent properties of the various batches; maximum capacities of ~480 mg I/g sorbent have been observed under static conditions (Matyas et al. 2021). Under typical flowing thin-bed testing conditions, loadings of 220–250 mg I/g AgAero are common.

2.2 ORNL TEST SYSTEMS AND METHODS

As stated previously, organic iodide sorption was evaluated at ORNL by using two types of test systems. The first test system is a custom-built TGA that contains thin beds of sorbent and is used to evaluate sorbent mass gain under a flowing gas stream. Thin-bed tests are typically one to three sorbent particles deep. Thin-bed testing is designed so that the sorbate concentration gradient across the sorbent thin bed can be assumed as constant. The second test system is a deep-bed column system and is used to evaluate sorbent aging, penetration of sorbate into the sorbent bed, and sorbate or analyte breakthrough.

2.2.1 Thin Bed Test System

The TGA built at ORNL for testing sorbents in flowing gas conditions produces loading rate data and total sorbent capacity under varying conditions (Figure 2). A custom manifold upstream of the TGA allows various components to be valved into the simulated off-gas stream (Figure 3). This includes NO_x gasses, which are expected to be present at 1–2 vol % in the DOG. Cylinders of gaseous NO and liquid N_2O_4 heated to promote the disassociation to gaseous NO_2 are procured commercially from AirGas and are contained within a regulated gas cabinet. Humid air is generated by sparging liquid water with a dry gas stream at a known flow rate and temperature for a total gas stream dew point of -70, 0, or 10°C.

All flow rates are regulated with Sierra Mass Flow controllers that display the active flow rate for monitoring. Standard tests are run at a superficial velocity of 10 m/min, which is equivalent to a volumetric flow rate of 11.51 slpm through the TGA chamber. Standard tests are run with the sorbent and gas stream heated to 150°C; however, some tests vary sorbent temperature between 135 and 165°C.

Between 1.8 and 2.0 g of sorbent are used for thin-bed tests. The circumference of the TGA basket is ~1 in (2.54 cm) (Figure 2). When using AgZ, the sorbent bed is typically one to three pellets deep. The sorbent is dried at testing temperature with dry air (-70°C dew point) overnight before I loading. This removes physisorbed water and ensures a stable initial weight. At this point, I and any other gas components are valved into the system. An example of raw TGA loading rate data and the calculated mass gain is presented in Figure 4. Raw mass data are collected by the data acquisition system at 1 min intervals, and the mass gained in milligrams of I per gram of sorbent is calculated at each time interval (T_x) relative to the time when I flow was initiated (T_0), per Eq. (1). Sorbent capacity is typically reached on the timescale of days to weeks, depending on the gas inlet I concentration. By tracking the sorbent weight during initial pretest drying, I sorption, and posttest purging, these tests not only measure I loading but also whether there is any measurable weight loss during pretest drying and posttest purging. Any weight loss during posttest purging indicates the presence of weakly held physisorbed I or another physisorbed species. The maximum amount of chemisorbed I (i.e., the sorbent capacity) is represented by the amount of weight gain after posttest purging.

$$10^3 \times \frac{Mass_{T_x} - Mass_{T_0}}{Mass_{T_0}}. \quad (1)$$

Figure 2. The ORNL TGA thin bed. The arrow points to the bed that contains iodide-loaded AgZ (green pellets).

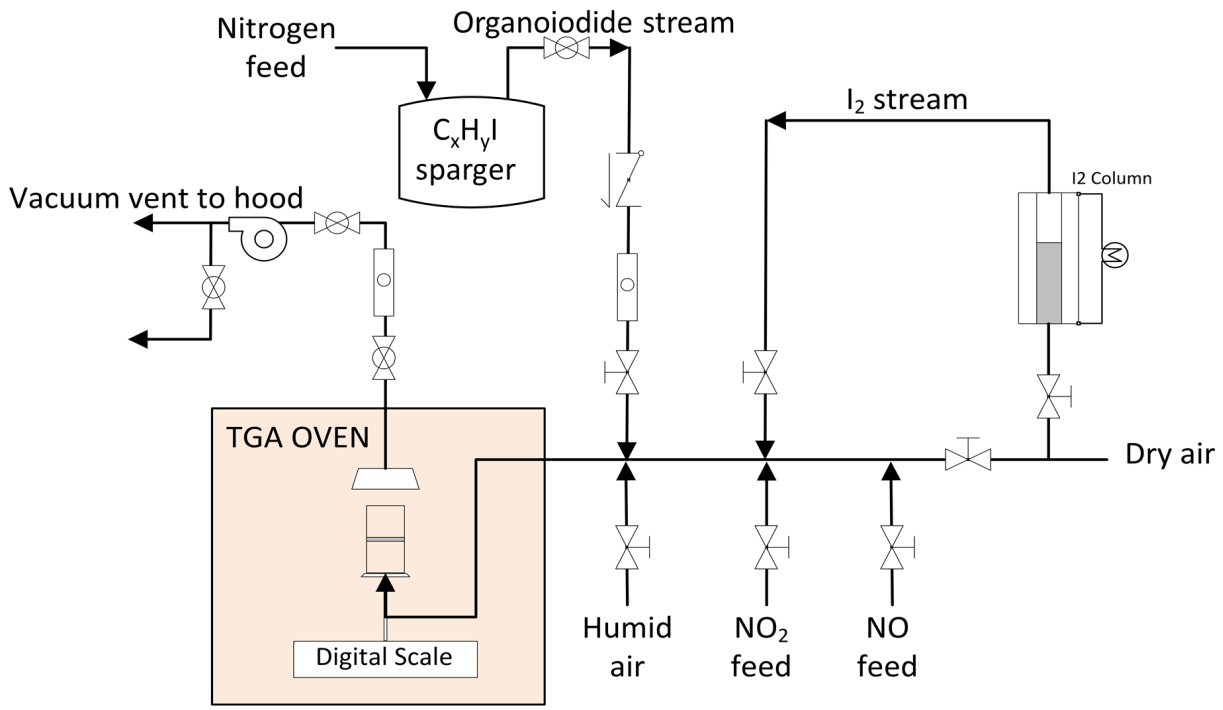

Figure 3. Simplified schematic of the ORNL TGA and associated manifold.

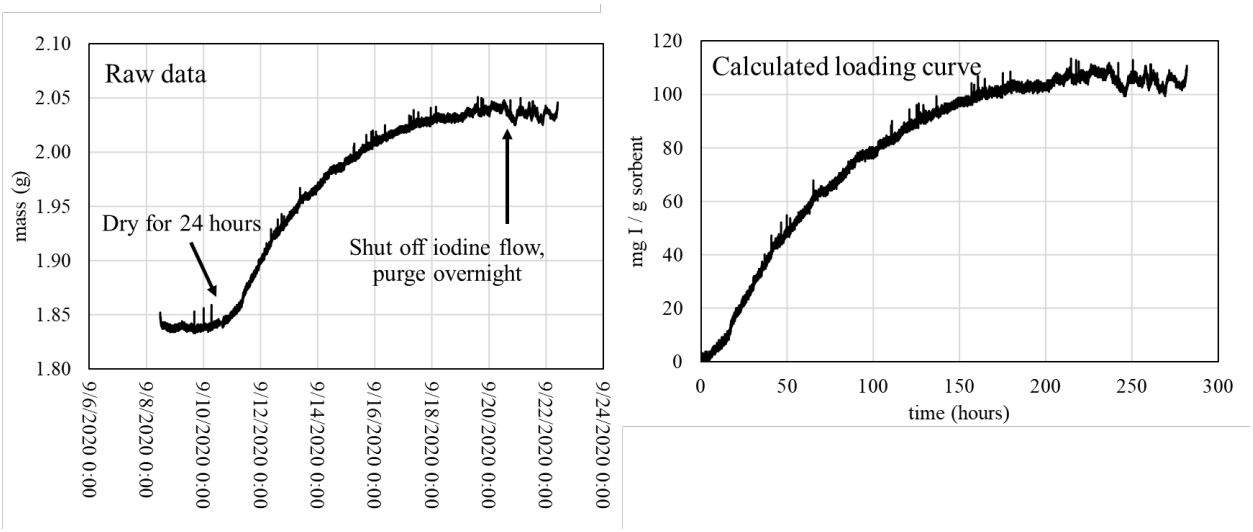

Figure 4. Example of raw TGA data and the calculated mass gain in milligrams of I per gram of sorbent.

2.2.2 Deep Bed Tests

Deep-bed testing systems at ORNL are designed to evaluate the mass transfer zone (MTZ) of I within a sorbent bed, the time to analyte breakthrough, the effects of flow rate on MTZ, and the effects of long-term aging on the sorbent. In contrast to INL deep-bed test systems, ORNL deep-bed test systems do not typically include effluent monitoring by GC with a flame ionization detector (FID). Deep-bed tests at ORNL typically target low concentration gas streams and run times that last weeks to months. Test systems use 1 in. (2.54 cm) inner diameter (ID) columns filled with sorbent (1–10 in. deep beds) in an

oven at 150°C. Upstream from the deep-bed oven, various Kin-Tek gas generators, organic iodide spargers, or humid air can be valved into the system.

2.2.3 Gaseous I Generation

Organic iodide-bearing gas streams were generated at by sparging liquid CH_3I, C_4H_9I, or $C_{12}H_{25}I$ with N_2 at a set flow rate or with a Kin-Tek gas generator by using permeation tubes with a set emission rate. The volatilization rate for liquid sparging was calculated by assuming that the sparging stream was saturated upon exiting the liquid and thus the concentration could be determined by using tabulated Antoine coefficients (Table 3). The CH_3I sparger was contained within a freezer kept at -33 or -40°C, depending on the desired concentration, to depress the vapor pressure to the levels required for generating low-concentration gas streams. The C_4H_9I sparger was kept at room temperature (20–22°C). The $C_{12}H_{25}I$ sparger was heat taped and insulated to run at 75°C. Both ORNL and INL encountered difficulty generating constant streams of $C_{12}H_{25}I$, given the low volatility. As is shown in several loading curves, the $C_{12}H_{25}I$ sparger design resulted in an initial burst of I in several tests at ORNL.

Inorganic I-bearing streams were generated by flowing a known flow rate of dry air through a column of I crystals kept at 18°C with a water bath.

Table 3. Organic iodide Antoine coefficients and calculated vapor pressure (mmHg) at STP. *Coefficients for (a) are from the NIST webbook calculated from Stull, 1947 and (b) are from Li and Rossini (1960).*

Coefficient	I_2[a]	CH_3I[a]	CH_3I[b]	C_4H_9I[b]	$C_{12}H_{25}I$[b]
A	3.36429	4.1554	6.8799	6.82262	7.229
B	1039.16	1177.78	1093.235	1358.86	2089.47
C	-146.58	-32.058	230.94	214.2	182.3
VP (mmHg)	0.242	402.0	405.9	13.86	0.001

2.2.4 ORNL Analytical Methods

Apparent I loadings reported based on TGA data could reflect weight gain from non-I compounds (e.g., water). TGA capacity estimates are validated by using neutron activation analysis (NAA), which is I specific. NAA is performed at the High Flux Isotope Reactor at ORNL. A ~0.2 g aliquot of the sorbent is used for analysis. The small sample size can exacerbate heterogeneities in the I-loaded bed, especially for deep-bed tests. The variability of one 0.2 g subsample from the larger 5–8 g sample was previously determined to be ~12–27% for subsamples that represented 2–3% of a large deep bed and ~10% for subsamples that represent thin beds (Jubin et al. 2017). To account for this, replicate samples are analyzed, when possible. Samples that were not analyzed with replicates might have added error due to this heterogeneity. NAA detection limits for I concentration range from ~5 to 50 ppmw, depending on the neutron flux used for the analyses. Total I loading is presented in milligrams of I per gram of sorbent.

Effluents downstream from the sorbent beds can be monitored for analyte breakthrough and reaction product formation by using GC-MS. An Agilent 8890 GC is coupled to an Agilent 5977B MS with a DB624-UI column (30m x 0.25mm ID). This is a 50% phenyl–50% methylpolysiloxane column designed to analyze volatile species. The GC method was designed to capture organic iodides ranging from methyl iodide to dodecyl iodide. The GC inlet temperature remains at 250°C while the column temperature starts at 30°C for 5 minutes before ramping to 220°C at a rate of 10°C/minute, then holding at 220°C for 6 minutes. Helium is used as the carrier gas with a constant flow rate of 1.2 ml/min. Gas tight syringes are used for direct sampling and introduction into the GC inlet. Sample volumes are typically 200 µL. Gas-

phase calibration standards were created by using the same sampling methods as the experiments. Standards were created at 1, 10, 50, and 100 ppm (Figure 5, 1 ppm C_4H_9I not shown). Peak areas integrated by the Agilent MassHunter software are used for quantification. Limits of detection (LODs) and limits of quantification (LOQs) were determined for each species by using chromatograph baseline statistics and regression statistics from the calibration curve generated by the standards. Detection limits are typically ~1 ppm for CH_3I and C_4H_9I.

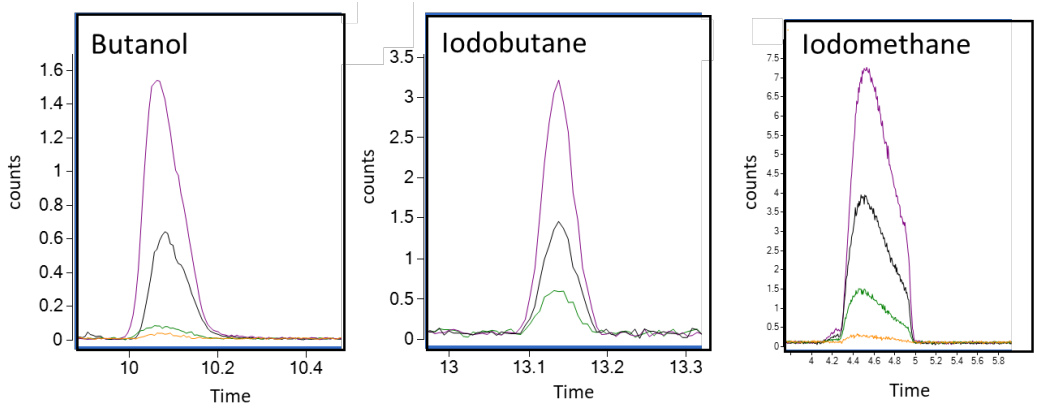

Figure 5. Examples of gas phase standard peaks on the GC chromatograph. The *y*-axis is the counts (not to scale between figures), and the *x*-axis is time. The purple, black, green, and orange lines represent 100, 50, 10, and 1-ppm concentrations, respectively, for the analyte of interest.

Scanning electron microscopy (SEM) was used to examine the loaded AgZ by using the Low Activation Materials Design and Analysis Laboratory group instrumentation at ORNL. AgZ pellets were mounted in epoxy and polished down 0.5 µm. Energy dispersive x-ray spectroscopy (EDS) on a TESCAN MIRA3 SEM was used to generate I and Ag distribution maps on organic iodide-loaded sorbent. Secondary electron (SE) and backscattered electron (BSE) images were collected with a 20.0 kV accelerating voltage.

2.3 IDAHO NATIONAL LABORATORY EXPERIMENTAL DESIGN

Deep-bed testing is performed at INL to assess MTZ, DFs, and sorbent capacities associated with various I-sorbent combinations, and the effects of various gas stream components on sorbent aging. These deep beds can be exposed to humid air, NO_x, and I generated for the VOG tests by using permeation tubes (Figure 6). The glass columns that contain the sorbent range from 0.75 to 1 in. ID (1.9 to 2.54 cm). Tests can be run with segmented sorbents beds separated by glass frits or as one continuous sorbent bed; total bed lengths are nominally about 8 in. deep (Soelberg et al. 2018, 2021). I concentration on the loaded AgZ is determined by using SEM EDS.

Effluents downstream from the deep bed can be monitored by using GC FID analysis at INL. This GC analysis allows for analyte breakthrough and reaction product detection down to 10 ppb (detection limit for CH_3I). A Hewlett Packard 5890 GC equipped with an RTX-624, 30 m × 0.32 mm ID, 1.8 µm DF column, and an FID is used for direct sampling with Supelco 75 µm carboxene/polydimethylsiloxane solid phase micro extraction (SPME) fibers. When peak identification is needed, a Shimadzu GC2010 with GCMS-QP2010 (with autosampler) is used with a J&W Scientific DB-1 (dimethyl polysiloxane) column (30 m × 0.25 mm ID × 1 µm) (Soelberg et al. 2018, 2021). By carefully monitoring the inlet and outlet concentrations of I, time-to-breakthrough and overall DFs can be established.

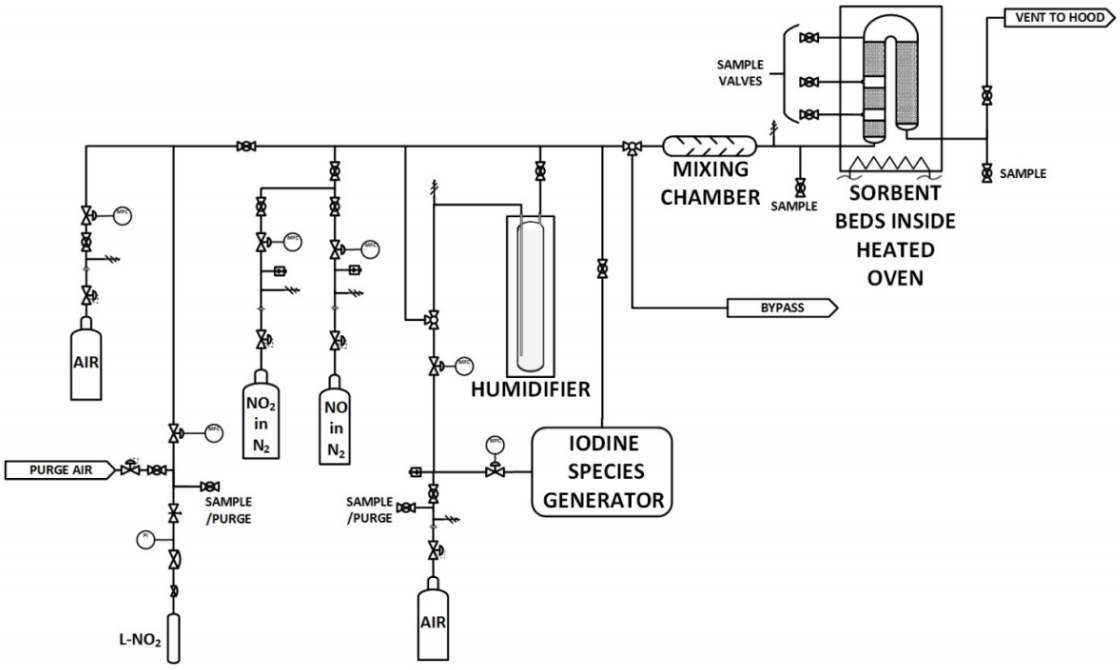

Figure 6. Schematic of Deep Bed test design at INL (figure from Soelberg et al., 2018).

3. ORNL EXPERIMENTAL EFFORTS IN 2021

3.1 EXPERIMENTAL GOALS

To accomplish the first objective of this report, ORNL performed a significant amount of experimental testing in 2021 aimed at better understanding fundamental and applied aspects of organic iodide capture by AgZ. Much of the applied testing was guided by the *Joint Test Plan for the Evaluation of I Retention for Long-Chain Organic Iodides* developed by INL and ORNL in 2018 and represented the conclusion of the collaborative testing effort between the two labs (Jubin et al. 2018). Initial results from this joint testing were documented in Bruffey et al. (2019) and were focused on the effects of organic iodide speciation and concentration on sorbate sorption by AgZ. More fundamental testing was performed in to understand whether the reaction pathways governing CH_3I sorption by AgZ could be translated to other organic iodide species. Initial results from that effort are documented in Greaney and Bruffey (2021) and are updated here.

The experimental test plan outlined here was designed to answer outstanding questions from the joint test plan (Jubin et al. 2018). These data are used in conjunction with data collected in recent years at INL and ORNL to develop a comprehensive understanding of organic iodide behavior in off-gas.

3.2 DESCRIPTION OF TESTING STRUCTURE

Recent testing at ORNL had four key thrusts. First, measure sorption rate and AgZ capacity for CH_3I, C_4H_9I, and $C_{12}H_{25}I$. Second, address the effects of gas velocity on the sorption of CH_3I and C_4H_9I by AgZ. Third, determine whether extended online time degraded sorbent capacity through aging. Fourth, assess sorption pathways for C_4H_9I by AgZ. Each of these thrusts is described individually here.

3.2.1 Sorption Rate and Loading Capacity

To answer the first four questions of the joint test plan, TGA thin-bed tests were used to measure the loading rate and sorbent capacity of CH_3I, C_4H_9I, and $C_{12}H_{25}I$ on AgZ. The planned test matrix is shown in Table 4.

Table 4. Test matrix for sorption rate and loading capacity.

Test #	Sorbent	Species	Concentration (ppm)	Temperature (°C)	Dew point (°C)
1	AgZ	CH_3I	50	150	-70
2	AgZ	CH_3I	50	150	0
3	AgZ	CH_3I	10	150	-70
4	AgZ	CH_3I	5	150	-70
5	AgZ	C_4H_9I	50	150	-70
6	AgZ	C_4H_9I	50	150	0
7	AgZ	C_4H_9I	10	150	-70
8	AgZ	C_4H_9I	5	150	-70
9	AgZ	$C_{12}H_{25}I$	50	150	-70
10	AgZ	$C_{12}H_{25}I$	10	150	-70
11	AgZ	$C_{12}H_{25}I$	5	150	-70
12	AgZ	I_2	25	150	-70
13	AgZ	I_2	5	150	-70

This test matrix evaluates the sorption of these three organic iodides and inorganic I by AgZ across concentrations of 5–50 ppm. The higher bound is more reflective of DOG I concentrations than of VOG I concentrations. The lower bound was established as a practical limit to the duration of each individual test; lower concentrations require months to achieve sorbent saturation. Although these concentrations are higher than those expected in the VOG, they allow for benchmarking sorption rate curves and AgZ capacity that can be extrapolated to lower concentrations. I_2 was included in these tests for comparison purposes. The planned molar concentration of I_2 is half that of the organic iodides to normalize the number of moles of I present in each molecule. The effects of water on organic iodide loading were also evaluated for CH_3I and C_4H_9I. Water will be present in both the DOG and VOG and was previously found to significantly affect the rate of CH_3I sorption by AgZ (Greaney and Bruffey 2020).

3.2.2 Effects of Gas Velocity

Most ORNL TGA testing was performed with a gas velocity of 10 m/min. Thus, four tests were designed to determine the depth of the MTZ under 1 m/min and 20 m/min flow velocities for CH_3I and C_4H_9I (Table 5).

Table 5: **Tests completed examining the effect of flow velocity on organic iodide sorption by AgZ.**

Test	Species	Flow velocity (m/min)	Concentration (ppb)	Duration (h)	I delivered (mg)
FVM-1-24	CH_3I	1	1060	574	120

FVM-20-1	CH_3I	20	1100	28.5	122
FVB-1-28	C_4H_9I	1	91	669	11.9
FVB-20-28	C_4H_9I	20	53	669	140
FVB-20-1	C_4H_9I	20	59	32	7.5

In these tests, a 15 cm deep (5.9 in) sorbent bed was contained in a 2.54 cm (1 in) wide column held constant at 150°C in an air gas stream with a 0°C dew point. Spargers were used to generate the organic iodide gas stream. Dilution with a slip stream design provided the final desired test concentration. An example of the system design and flow rates used in the 1 m/min CH_3I tests are shown in Figure 7. The generated C_4H_9I concentration was calculated to be 59 ppb for the 20 m/min test (32 h or ~1 day) and 91 ppb for the 1 m/min test (669 h or ~28 days). The generated CH_3I concentration was calculated to be 1 ppm for the 20 m/min test (28 h or ~1 day) and 1 ppm for the 1 m/min test (574 h or ~24 days) (Table 5). The duration of the 1 m/min test vs. 20 m/min test was chosen to normalize the mass of CH_3I or C_4H_9I delivered to the bed. Thus, for both gas velocities, roughly the same mass of iodide was introduced to the sorbent bed.

An additional 53 ppm C_4H_9I test (FVB-20-28) was run at 20 m/min for the same duration as the 1 m/min test (669 h or ~28 days) (Table 5). Although this test resulted in a greater mass of I adsorbing to the bed than the 1 m/min test, these data can be used to understand the penetration depth of organic iodides in a higher flow velocity during longer time frames.

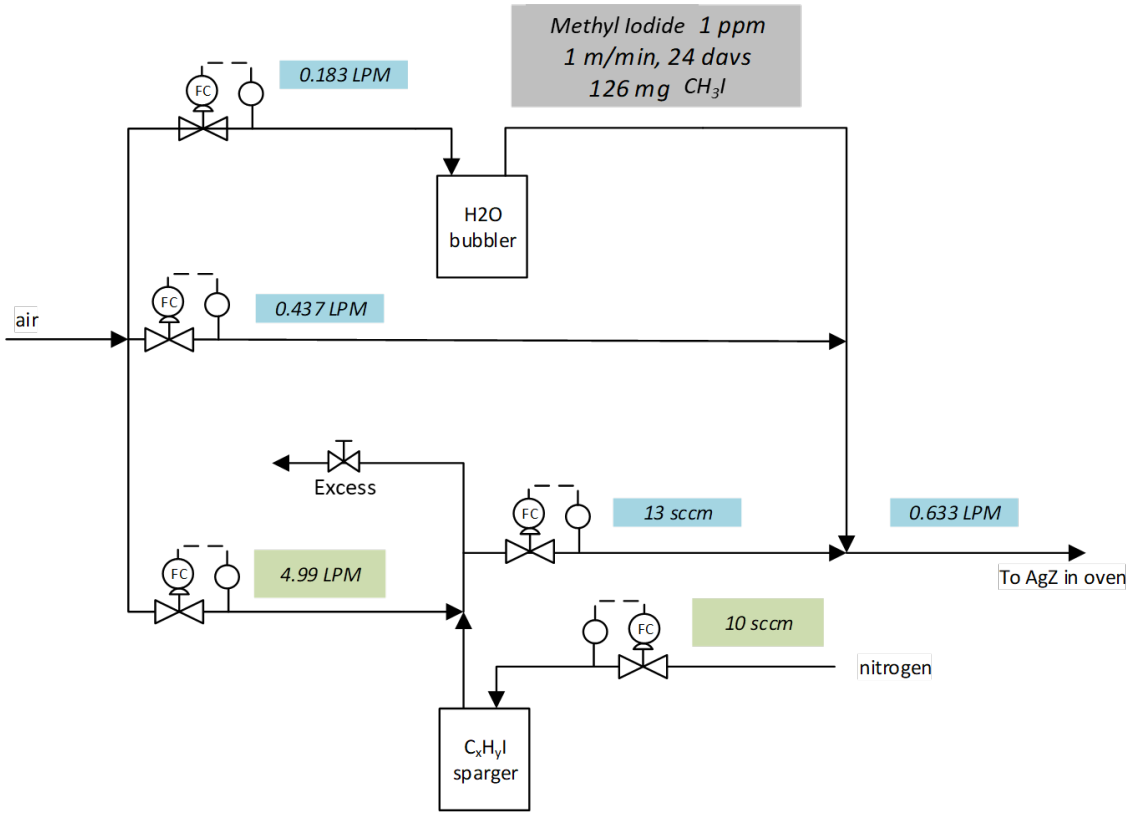

Figure 7. Example flow diagram of the 1 m/min CH_3I flow-rate test designed with a slip stream to generate low concentration organic iodide streams.

3.2.3 Effects of Sorbent Aging

As reduced AgZ is exposed to air and humidity, the capacity for I sorption decreases (Bruffey et al. 2017, Jubin et al. 2015). Sorbent aging is often attributed to the oxidation of the Ag within the mordenite, which makes the formation of AgI or $AgIO_3$ thermodynamically unfavorable. To better understand how sorbent aging effects could vary based on I speciation, the capacity of 9 month-aged AgZ for CH_3I, C_4H_9I, and $C_{12}H_{25}I$ was determined through thin-bed testing. The AgZ used in these experiments was aged for 286 days in a humid gas stream (0°C dew point) at a temperature of 150°C (Jubin et al. 2018). The capacity of this AgZ for CH_3I and C_4H_9I was determined by using previously described testing conditions (Section 2.2.1) with sorbate concentrations of 50 ppm in the feed gas stream. AgZ capacity for $C_{12}H_{25}I$ was determined by using a concentration of 25 ppm in the feed stream. Because of limited TGA availability, the CH_3I and C_4H_9I tests were completed in a 1 in. column held at 150°C. Thus, loading curves are not available for these species. The $C_{12}H_{25}I$ test was completed in the TGA as a standard thin-bed test.

3.2.4 Butyl Iodide Sorption Pathway Analysis

To determine whether C_4H_9I is sorbed by AgZ through reaction pathways similar to CH_3I, multiple tests were conducted to monitor the effluent downstream of an AgZ bed for reaction products. Butanol, C_4H_9OH, was the primary reaction product that was hypothesized to form following reactions proposed by Chebbi et al. (2016) and Nenoff et al. (2014). Both thin- and deeper-bed tests were completed in a 1 in. column in an oven. The nominal superficial velocity used for all tests was 10 m/min at 150°C. Both humid and dry air were used. C_4H_9I was generated upstream of the oven from a liquid sparger by bubbling air at a set flow rate and temperature. The effluent downstream of the sorbent bed was monitored by GC-MS for C_4H_9I and any reaction products that may form (specifically, C_4H_9OH). Additionally, two tests were completed to test C_4H_9OH sorption on AgZ. One test was completed in the 1 in. column oven, and one was completed in a TGA.

3.3 RESULTS OF ORNL 2021 EXPERIMENTATION

The experimentation completed at ORNL in 2021 resulted in a wealth of data characterizing many facets of organic iodide sorption from dilute gas streams. Results and initial conclusions are provided here and expanded upon in Section 4.

3.3.1 Total sorbent capacity as a function of iodine speciation

Sorbent capacity tests completed between 5 and 50 ppm resulted in sorbent saturation (as observed by stabilized sorbent weight) for only the higher concentration tests (Table 6). Figure 8 shows the loading curves for CH_3I, C_4H_9I, $C_{12}H_{25}I$, and I_2 at 50 ppm sorbate concentration in the feed stream. In these tests, the capacity of AgZ for each of the three organic iodide species was statistically indistinguishable and roughly equal to 100 (±10) mg I/g AgZ. This capacity is the same as the I_2 capacity for an average batch of reduced AgZ (Figure 8). This is a notable finding because it indicates that the **AgZ saturation capacity is not dependent on I speciation at parts-per-million concentration ranges.**

Although mass gain recorded by the TGA appeared to plateau, a visual inspection of the AgZ pellets and an examination of the loading curves shown in Figures 9 and 10 suggest that the lower concentration tests (10 and 5 ppm, respectively) were stopped before the sorbent reached capacity. The maximum sorbent loading observed for CH_3I at 10 ppm sorbate concentration in the feed stream was 76.4 ± 7.6 mg I/g AgZ. For C_4H_9I, the maximum sorbent loading observed was 87.8 ± 8.8 and 92.7 ± 9.3 mg I/g AgZ for feed streams with 10 and 5 ppm sorbate concentration, respectively. The maximum sorbent loading observed for $C_{12}H_{25}I$ was 79.7 ± 8.0 and 40.5 ± 4.1 mg I/g AgZ for feed streams with 10 and 5 ppm sorbate

concentrations, respectively. At these lower concentrations, reaching full sorbent capacity could take weeks to months.

I_2 testing performed for comparison showed that sorbate concentrations of 50 and 5 ppm did not significantly affect AgZ saturation capacity with capacities of 85.5 ± 8.6 and 89.4 ± 8.9 mg I/g AgZ observed, respectively. I_2 testing by using 25 ppm I_2 in the feed stream had a discrepancy between TGA and NAA measurements, possibly attributable to a sampling error.

The silver-iodide species formed during organic iodide adsorption was not characterized with analytical methods. Both AgI and $AgIO_3$ are theorized to form (Table 2). However, stoichiometric calculations suggest that AgI would be the dominant species. If the AgZ pellets contain between 9.5 wt% and 11 wt% Ag, and the molar ratio of silver to iodide in AgI and $AgIO_3$ is 1:1, then the maximum iodide loading expected is roughly equivalent (~10 wt%) given the similar molecular mass of Ag (109 g/mol) and iodide (126.9 g/mol). This 1:1 Ag:I ratio is observed in the NAA data in Table 6 where the 50 ppm tests reached 106 mg I /g sorbent (10.6 wt%) to 119 mg I/g sorbent (11.9 wt%). If $AgIO_3$ formed, the estimate sorbent loading recorded by the TGA should be higher than the iodine content recorded by NAA. This is not the case for the organic iodides, where the ~50 ppm TGA data matches the NAA data. This suggests that AgI is the dominant species formed during iodine loading.

Table 6: AgZ capacity for organic iodides across a concentration range of 5–50 ppm sorbate.

Sorbent	Species	Concentration (ppm)	Temp. °C	Dew Point	TGA	NAA	Visual saturation?
				°C	(mg I / g sorbent)		
AgZ	C_4H_9I	42	150	0	110	110.9 ± 11.1	Y
AgZ	C_4H_9I	42	135	-70	104	114.8 ± 11.5	Y
AgZ	C_4H_9I	10	135	-70	58	60.7 ± 6.1	Y
AgZ	C_4H_9I	10	150	-70	83	87.8 ± 8.8	N
AgZ	C_4H_9I	5	150	-70	81	92.7 ± 9.3	N
AgZ	$C_{12}H_{25}I$	≤50	150	-70	110	112.0 ± 11.2	Y
AgZ	$C_{12}H_{25}I$	10	150	-70	90	79.7 ± 8.0	N
AgZ	$C_{12}H_{25}I$	5	150	-70	41	40.5 ± 4.1	N
AgZ	CH_3I	50	150	-70	111	106.6 ± 10.7	N
AgZ	CH_3I	10	150	-70	47	76.4 ± 7.6	N
AgZ	CH_3I	5	150	-70	80	*Not determined*	N
AgZ	I_2	50	150	-70	100	85.5 ± 8.6	Y
AgZ	I_2	50	150	-70	120	119.0 ± 11.9	Y
AgZ	I_2	25	150	-70	86	62.5 ± 6.3	N
AgZ	I_2	5	150	-70	89	89.4 ± 8.9	N

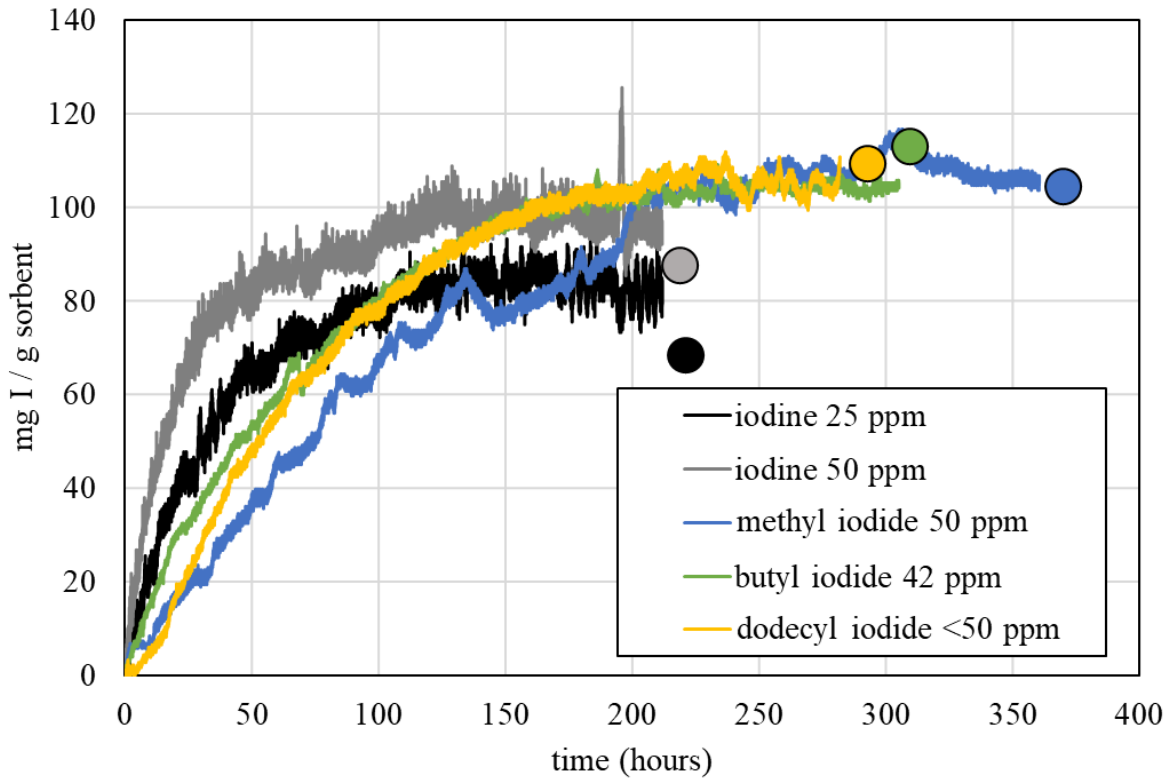

Figure 8. 50 ppm CH_3I, C_4H_9I, and $C_{12}H_{25}I$, and I_2 loading curves for AgZ. The circles indicate NAA data (mg I/ g sorbent).

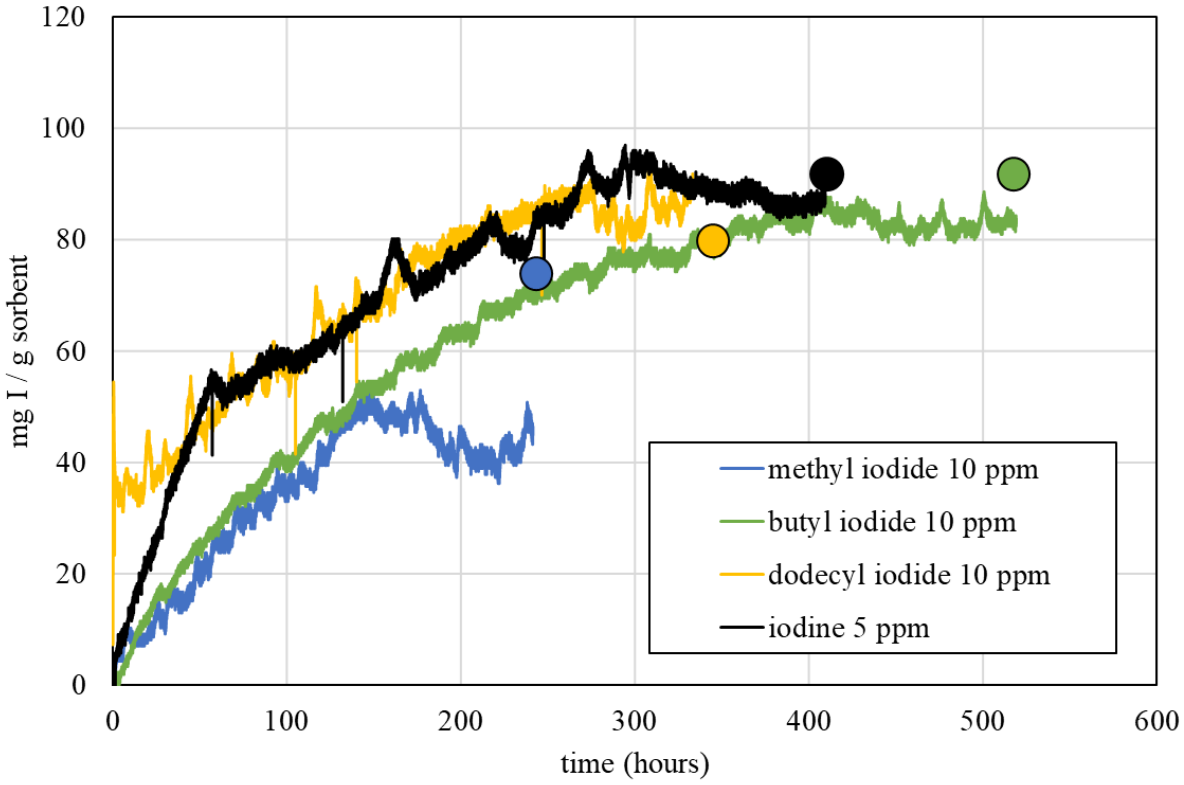

Figure 9. 10 ppm CH_3I, C_4H_9I, and $C_{12}H_{25}I$, and I_2 loading curves for AgZ; 5 ppm I_2 is equivalent to 10 ppm-mol of iodide. The circles indicate NAA data (mg I/ g sorbent). The delivery of 10 ppm $C_{12}H_{25}I$ to the TGA was characterized by an initial burst of $C_{12}H_{25}I$.

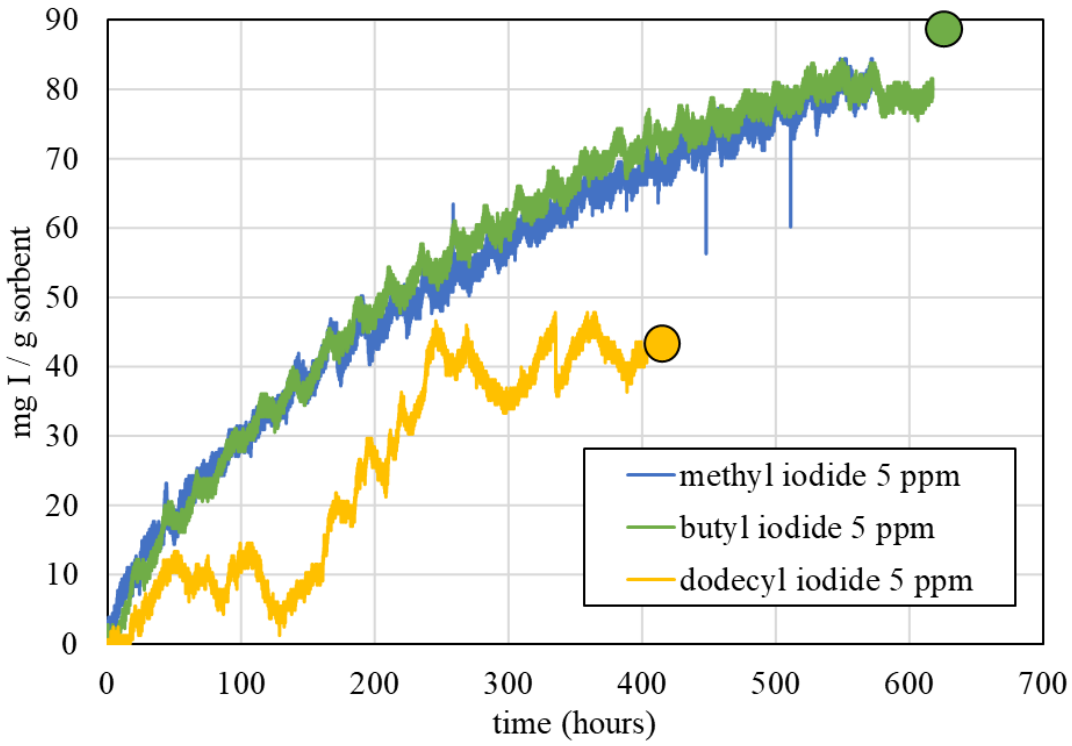

Figure 10. 5 ppm CH_3I, C_4H_9I and $C_{12}H_{25}I$ loading curves for AgZ. The circles indicate NAA data (mg I/g sorbent).

3.3.2 Sorption Rate as a Function of I Speciation and Concentration

The loading rate can be assessed in multiple ways (Table 7). A typical AgZ loading curve follows a logarithmic trend and as such can be subdivided into two stages: initial growth followed by a slowing asymptotic rate. Depending on I species, the inflection point tends to occur at around 50–100 h of loading for higher concentrations (50 ppm) and at around 300 h for lower concentration tests (5 ppm). To compare the loading rates between organic iodide species and concentrations, an initial loading rate and the time to sorbent saturation are calculated. The initial loading rate is calculated as the slope of the loading curve (mg I/h) between 10 and 40 h of loading. This time is chosen because all I species are in the first stage of loading at this time interval and because the large range accounts for variation in the curve induced by an uneven delivery stream (low concentration tests) and external variations induced by the balance (e.g., due to fluctuations in balance temperature and humidity). The time to sorbent saturation is calculated as the point on the loading curve at which the average loading over the next 24 h is less than the average loading of the previous 24 h. The total loading rate is calculated as milligrams of I per gram of sorbent gained once the sorbent reaches saturation.

The initial 10–40 h loading rate was found to be dependent on organic iodide species and concentration (Table 7). Intuitively, a higher organic iodide or I_2 concentration in the gas stream results in a faster initial loading rate (e.g., Figure 11, Figure 12, Figure 13, Figure 14) and achieves sorbent saturation more quickly than the lower concentration tests (Table 7). This is true for all organic I species studied and for I_2 (Figure 15). The total loading rate can be calculated for the varying concentrations of each iodide in the off-gas. The lower concentration tests (10 and 5 ppm) likely did not reach sorbent saturation, but an estimated loading rate can still be calculated. For C_4H_9I and $C_{12}H_{25}I$, an order of magnitude decrease in concentration (50 to 5 ppm), results in a 60–75% decrease in loading rate.

With a sorbate concentration of 50 ppm in the feed stream, the highest initial loading rate belongs to inorganic iodide (tested as 25 ppm I_2) followed by $C_{12}H_{25}I$, C_4H_9I, and CH_3I (Figure 16). The reverse is true for the time-to-saturation parameter. In a 50 ppm gas stream, I_2 reaches sorbent saturation the quickest, followed by the three organic iodides in order of increasing molecular weight (Figure 16). Inorganic iodide and CH_3I reach sorbent capacity at roughly the same time in a high concentration stream, but it takes twice as long for $C_{12}H_{25}I$ to saturate the AgZ thin bed.

Observations from this test matrix can be summarized by noting that the initial sorption rate increases with increasing organic iodide carbon chain length, but the rate tapers significantly so that the total loading rate increases with decreasing organic iodide carbon chain length. Smaller organic iodides saturate AgZ more quickly.

Table 7. **Initial loading rate and time to sorbent saturation for the organic iodides and iodine.** The 50 ppm test for C_4H_9I was actually closer to 42 ppm. The 50 ppm-mol I was run as a 25 ppm I_2 gas stream and the 10 ppm-mol I was run as a 5 ppm I_2 gas stream. The asterisk (*) denotes tests that might not have reached sorbent saturation.

	CH_3I	**C_4H_9I**	**$C_{12}H_{25}I$**	**I_2**
10 - 40 hour loading rate (mg I/g/r)				
50 ppm	0.66	0.95	1.20	1.74
10 ppm	0.32	0.48	0.21	0.93
5 ppm	0.32	0.34	0.31	--
Time to sorbent saturation (h)				
50 ppm	134	187	257	119
10 ppm	147*	309*	265*	164
5 ppm	570*	592*	268*	--
Total loading rate (mg I/g/h)				
50 ppm	0.64	0.56	0.42	0.70
10 ppm	0.35	0.26	0.33	0.48
5 ppm	0.14	0.13	0.16	--

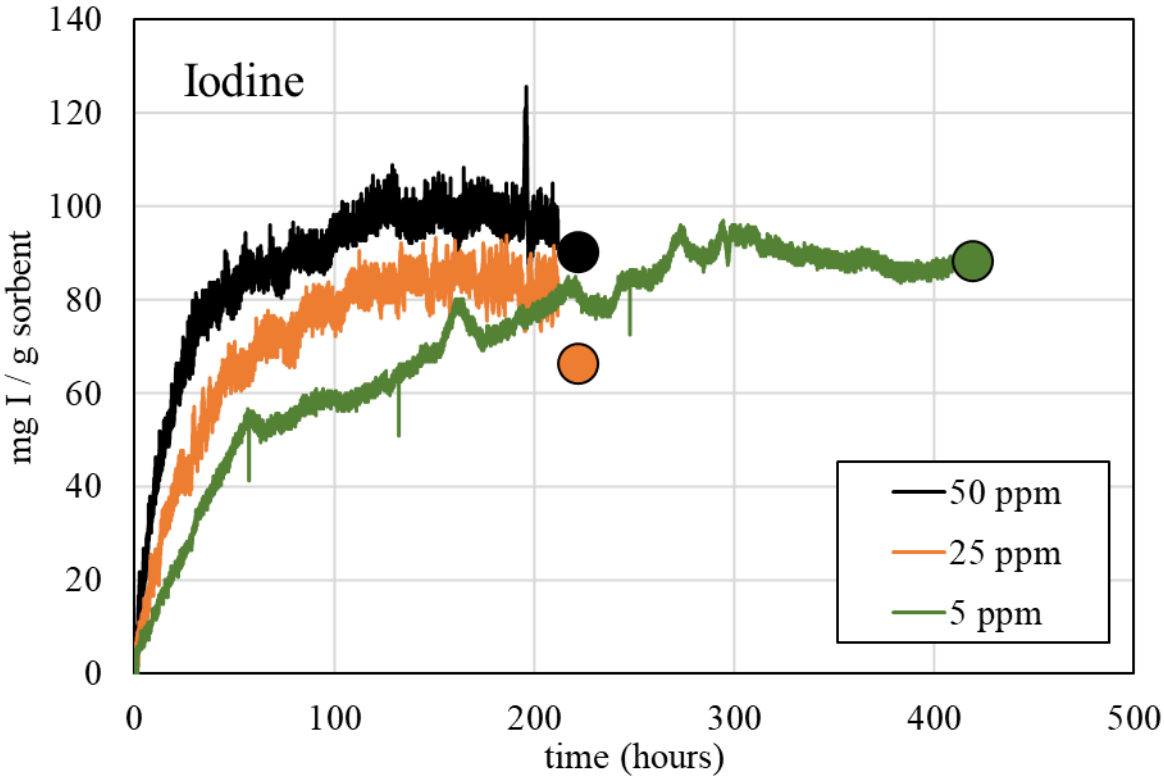

Figure 11. Effect of I_2 concentration on loading rate and sorbent saturation.

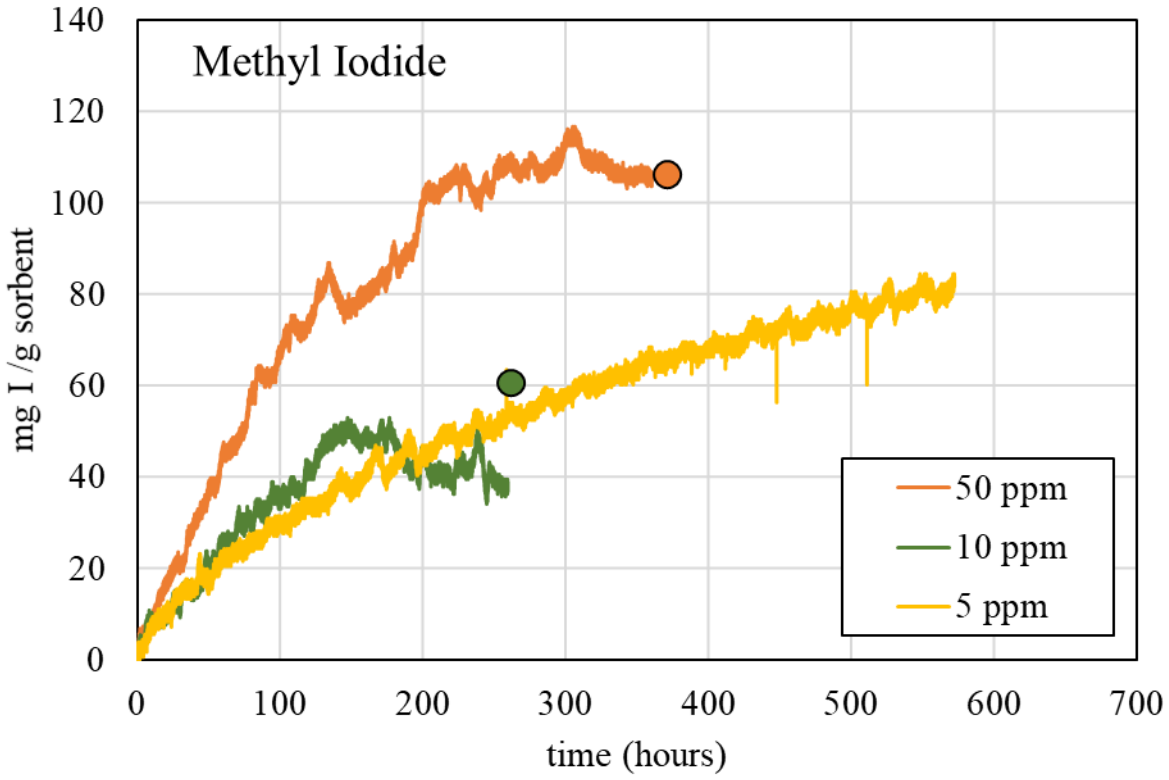

Figure 12. Effect of CH_3I concentration on loading rate and sorbent saturation. NAA data is not available for the 5 ppm test.

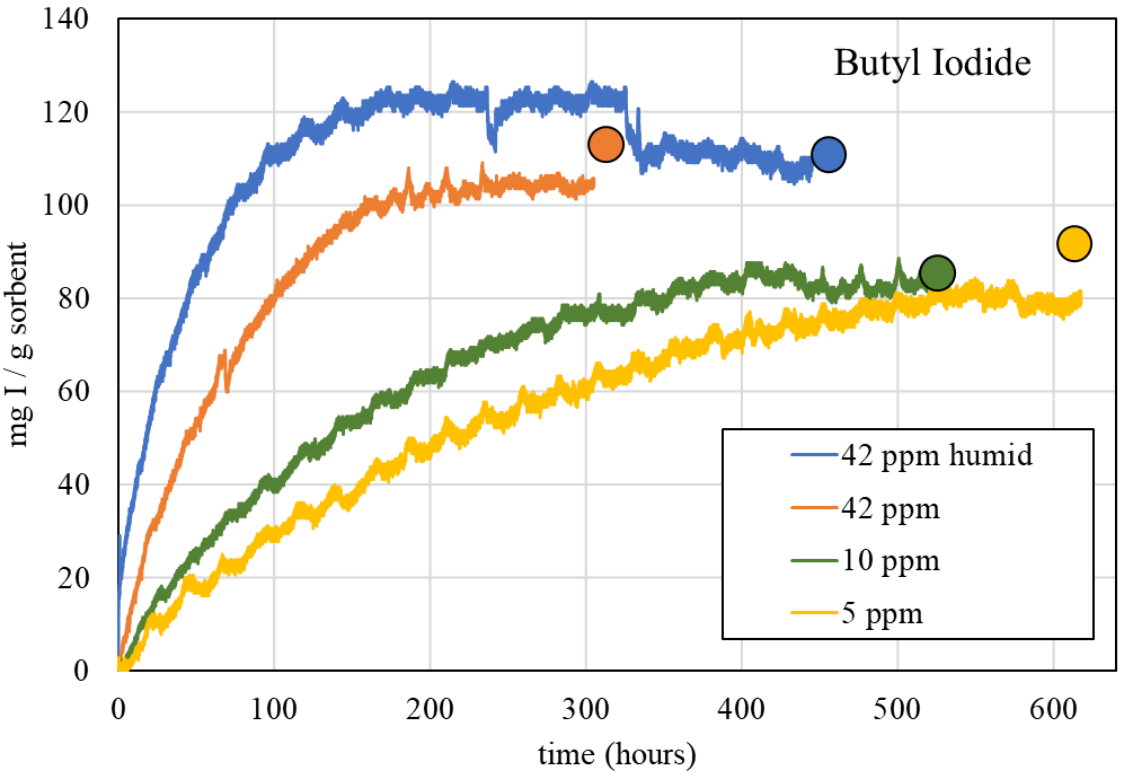

Figure 13. Effect of C_4H_9I concentration on loading rate and sorbent saturation.

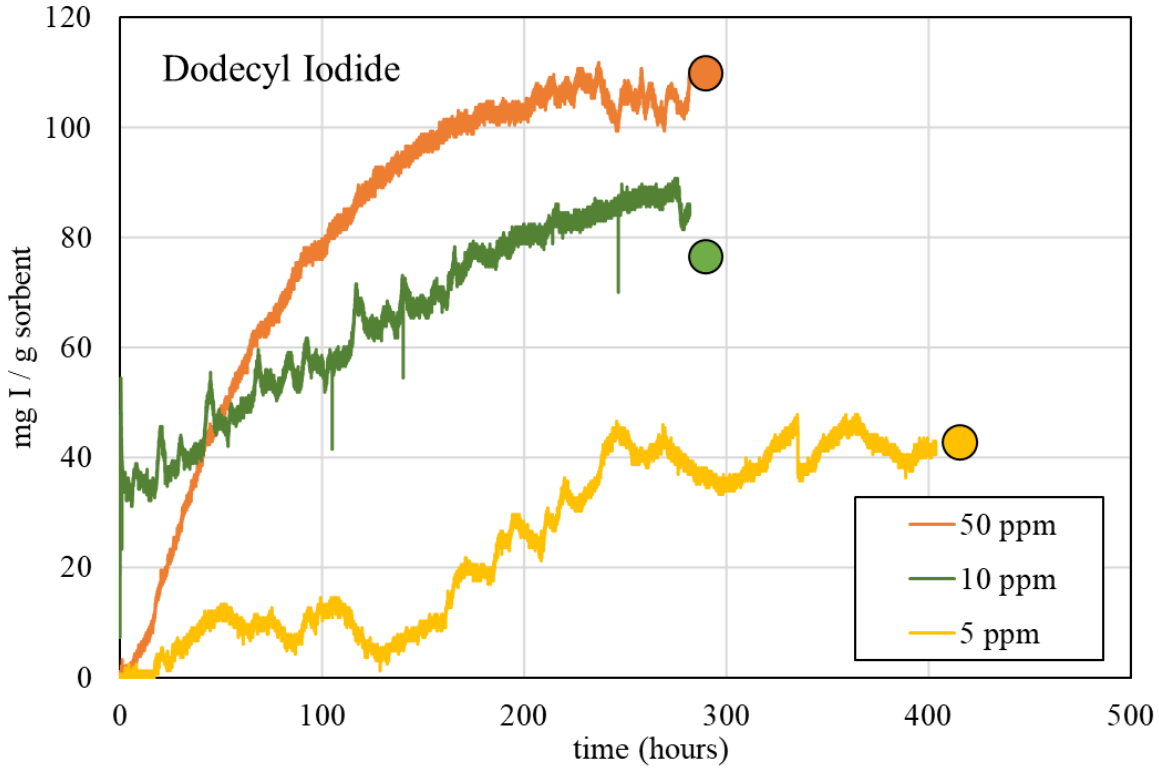

Figure 14. Effect of $C_{12}H_{25}I$ concentration on loading rate and sorbent saturation. The delivery of 10 ppm $C_{12}H_{25}I$ to the TGA was characterized by an initial burst of $C_{12}H_{25}I$.

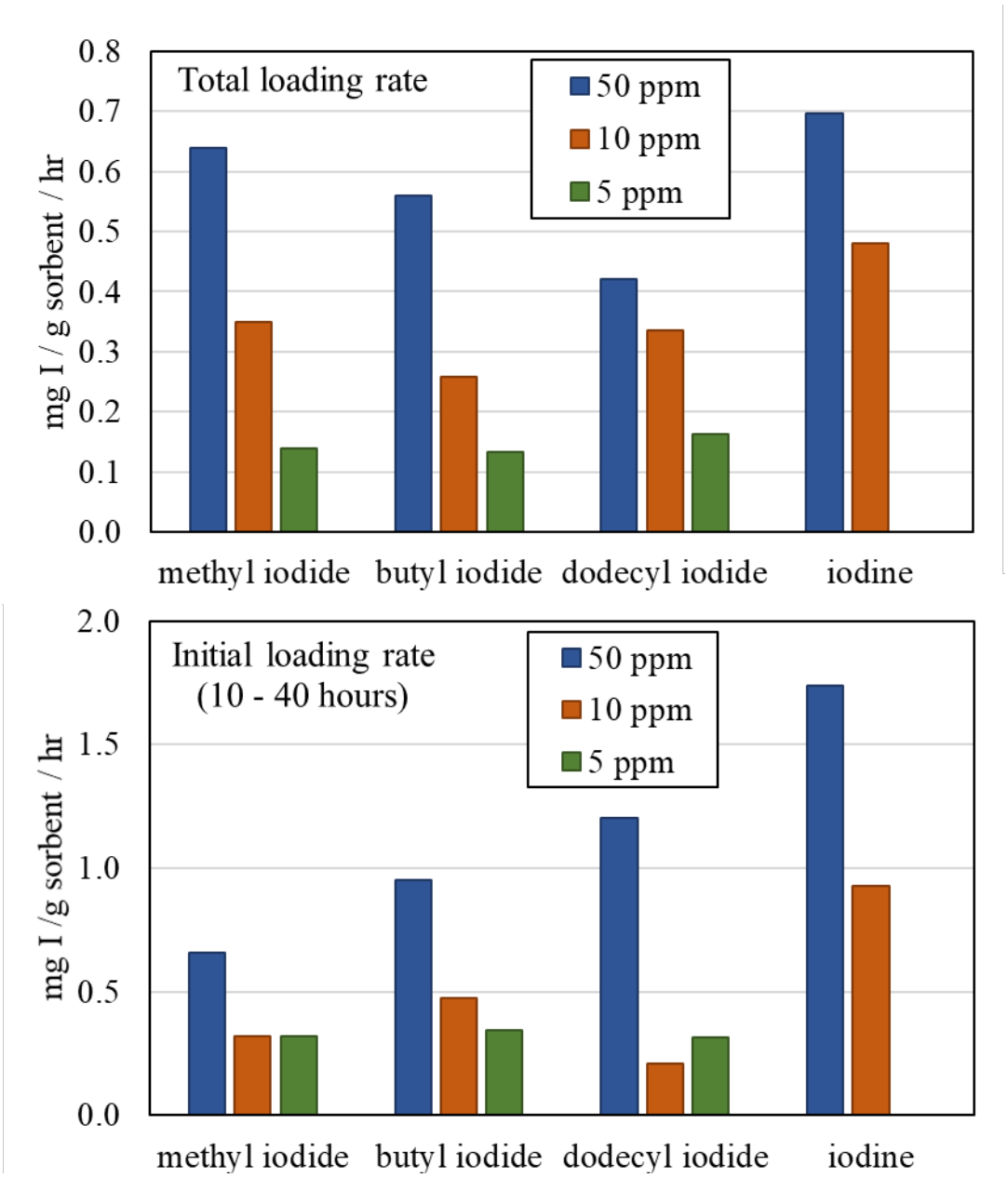

Figure 15. Initial (10-40 hour) and total loading rates in mg I/g sorbent/hour for the organic iodides and iodine.

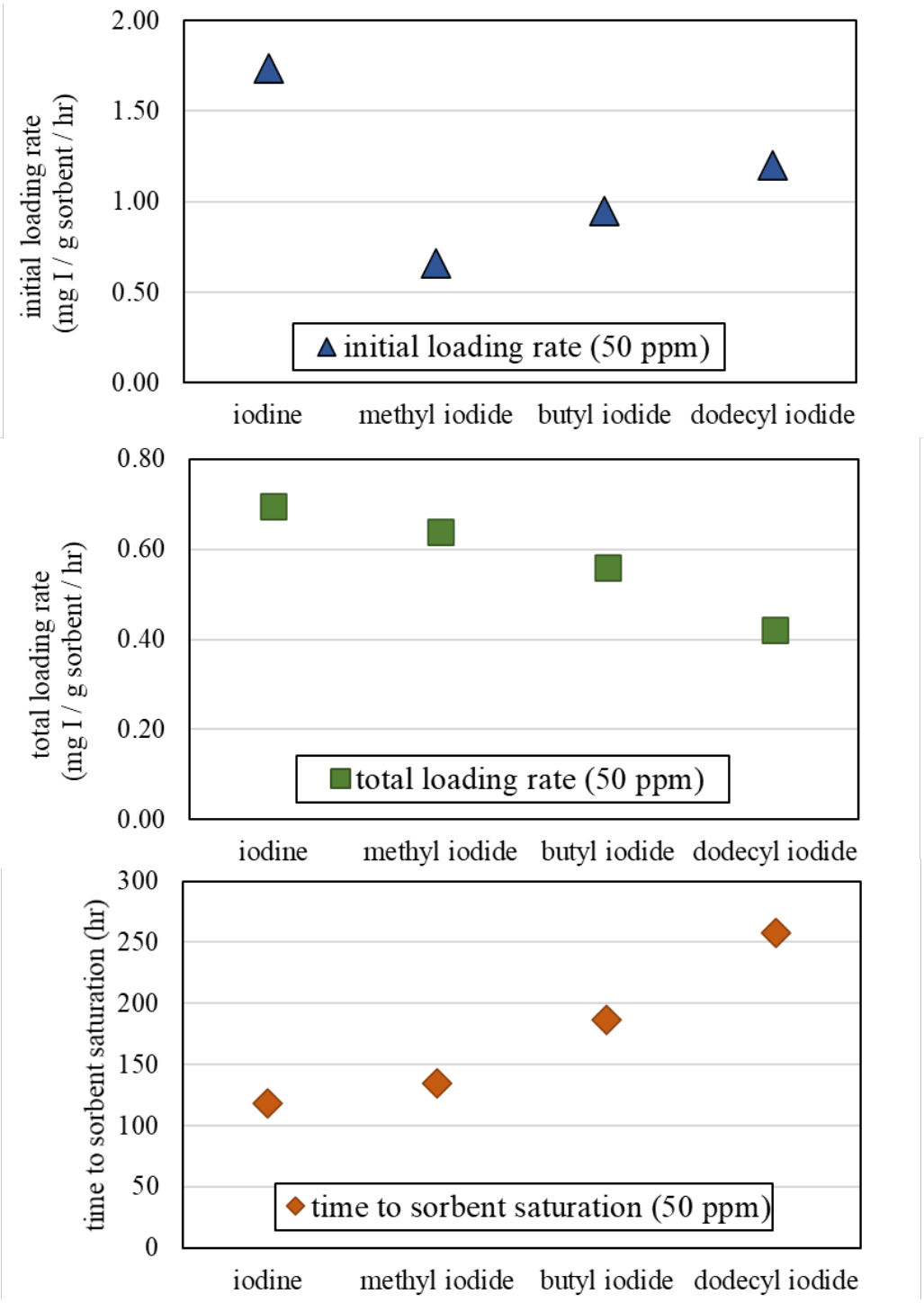

Figure 16. Comparison of the initial loading rate from 10 – 40 hours (mg I/g sorbent/h), total loading rate (mg I/g sorbent/h), and the time to sorbent saturation (h) for the organic iodides and I_2 (50 ppm).

3.3.3 Visual Saturation Observations

As I sorbs onto the mordenite, it forms AgI or $AgIO_3$, causing the sorbent to turn in a green-yellow color. Thus, I sorption is visually apparent, although a minimum detection limit or concentration measurement cannot be assessed for visual observation. To assist in observation, photomicrographs of cross-sectioned AgZ pellets were obtained for this series of testing.

The AgZ exposed to higher concentration I streams that reached apparent sorbent saturation on the TGA appears to be uniform in color (Figure 17). AgZ exposed to lower concentration gas streams (5 and 10 ppm) did not reach saturation, even after weeks of testing. The AgZ recovered from these tests showed that I was located only around the circumference of the sorbent (Figure 17).

Longer-chain iodide sorption appears to follow the shrinking core model previously proposed for I (Nan 2017) and CH_3I (Tang et al. 2020; Jubin 1994) sorption by zeolites. I diffusion into the AgZ pellet following a shrinking core model is visually apparent for C_4H_9I and $C_{12}H_{25}I$ (Figure 17). Initial I loading occurs around the circumference of the AgZ pellet, leaving an unreacted core. As the sorbent is exposed to additional sorbate, the reaction front moves toward the center of the pellet, resulting in the shrinking of the unreacted core. Figure 17 demonstrates a vanishingly small unreacted core as the sorbent nears saturation.

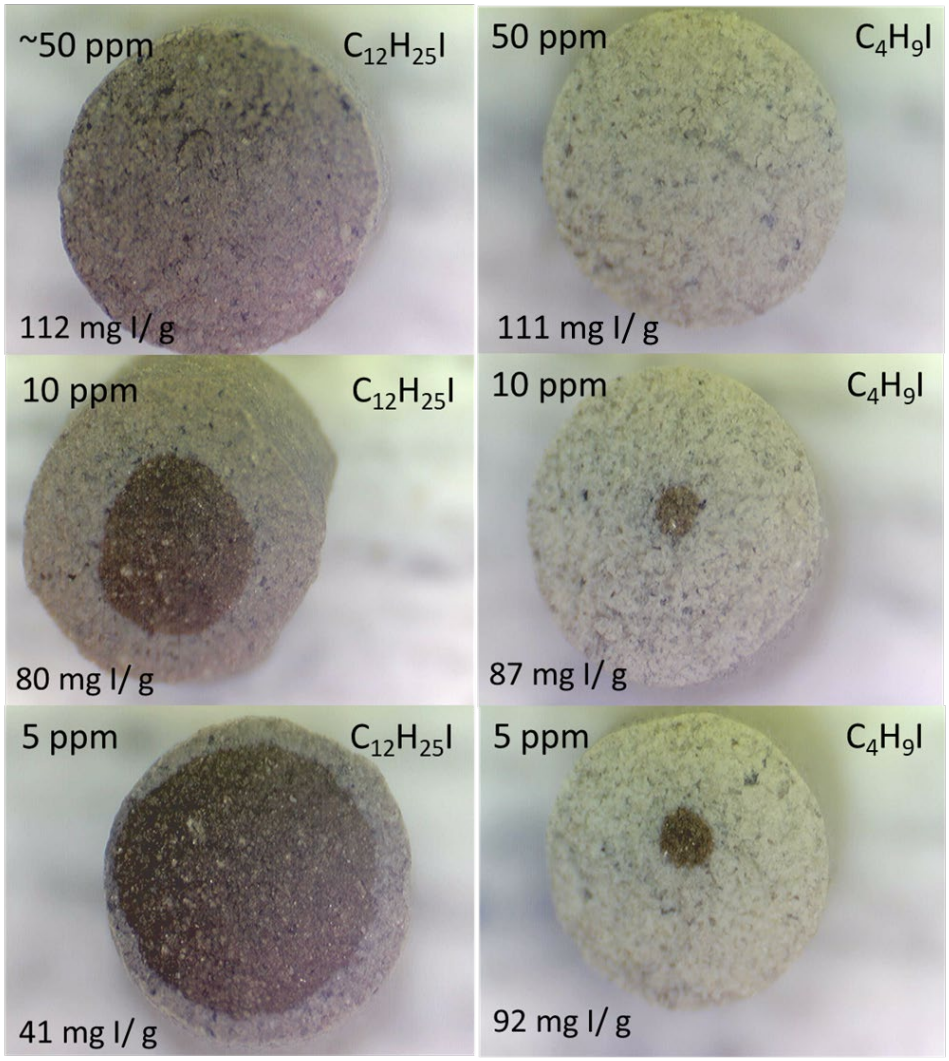

Figure 17. Photomicrographs of I loading along the C-axis cross section of AgZ pellets. These pellets were exposed to 50 ppm (top row), 10 ppm (middle row), and 5 ppm (bottom row) streams of $C_{12}H_{25}I$ (left) and C_4H_9I (right). The field of view is ~3 mm.

3.3.4 Effects of Gas Velocity on Organic Iodide Sorption

3.3.4.1 Methyl Iodide

One 1 m/min test and one 20 m/min test were performed to compare CH_3I loading on an AgZ bed as a function of the superficial velocity of the off-gas (Table 8). In test FVM-1-24, 119.3 mg of I were adsorbed to the 1 m/min bed over 574 h, and in test FVM-20-1, 122.1 mg of I were adsorbed to the 20 m/min bed over 28 h. The total mass of CH_3I captured on the beds is approximately 110% of the theoretically delivered mass for each test, indicating that all volatilized material were successfully sorbed by AgZ within measurement error. Because both sorbent beds received roughly the same mass of CH_3I, the loading profiles can be compared to determine the effect that superficial gas velocity has on profile geometry.

Significant variations in the I loading pattern were observed for the two tests, the primary difference being that the 20 m/min profile shows roughly even distribution across the bed, whereas the 1 m/min

profile shows a nearly exponential decrease in distribution across the bed (Figure 18). Over the course of 24 days, 1 ppm of CH_3I in the 1 m/min off-gas stream penetrated only ~5 cm (2 in.) into the bed with >99% of the I contained in the first 6 cm (2.4 in.). In contrast, over 28 h, 1 ppm of CH_3I in the 20 m/min off-gas stream penetrated through the 14 cm (5.5 in.) deep bed. In this test, only 47% of the I was contained in the first 6 cm. For comparison, the outlet segment (F) of the 20 m/min test contained 260 times more I than the outlet segment in the 1 m/min test. Additionally, in the last 2 h of the 20 m/min CH_3I test, a parts-per-billion-level breakthrough of CH_3I was observed at the bed outlet by using a GC-MS analysis of the effluent. This breakthrough was above the LOD but below the LOQ.

These data show that at a CH_3I concentration of 1 ppm, the flow velocity strongly affects the loading profile of a sorbent bed. A linear regression can be fit to the 20 m/min test loading profile which gives a slope of -0.21 mg I/g sorbent/cm (Figure 19). Using this slope to calculate where the x-intercept is zero, a 20 m/min 1 ppm loading rate would generate an estimated penetration depth at least 22 cm (8.7 in) long. The loading profile generated is not representative of a true MTZ because sorbent saturation was not reached at the inlet to the bed. Instead, the penetration depth is used to describe I movement through the bed. This estimated minimum penetration depth is two to three times longer than 1 ppm MTZs measured at 10 m/min (Soelberg et al. 2021) and more than four times longer than the 1 m/min penetration depth recorded here.

Table 8. Results of 1 ppm CH_3I flow-rate tests at 1 m/min (24 days) and 20 m/min (1 day).

AgZ segment	Segment position	Segment mass (g)	Segment height (cm)	Bed Depth (cm)	Total iodine (mg)	mg I / g sorbent	± 2σ (mg I/g sorbent)
1 m/min, 574 hours (~24 days), 1 ppm CH_3I							
FVM-1-24-A	inlet	5.56	1.85	1.85	92.2	16.6	0.19
FVM-1-24-B		4.16	1.39	3.24	25.4	6.10	0.07
FVM-1-24-C		6.16	2.05	5.29	1.80	0.29	0.01
FVM-1-24-D		5.62	1.87	7.16	0.06	0.01	0.01
FVM-1-24-E		6.28	2.09	9.25	0.02	0.00	0.00
FVM-1-24-F	outlet	12.84	4.28	13.53	0.09	0.01	0.00
	20 m/min, 28 hours (~1 day), 1 ppm CH_3I						
FVM-20-1-A	inlet	3.11	1.04	1.04	15.9	5.11	0.06
FVM-20-1-B		5.72	1.91	2.95	20.6	3.61	0.04
FVM-20-1-C		5.97	1.99	4.94	20.9	3.51	0.04
FVM-20-1-D		6.18	2.06	7.00	19.3	3.12	0.04
FVM-20-1-E		6.02	2.01	9.01	16.7	2.77	0.03
FVM-20-1-F	outlet	13.2	4.41	13.42	28.7	1.83	0.03

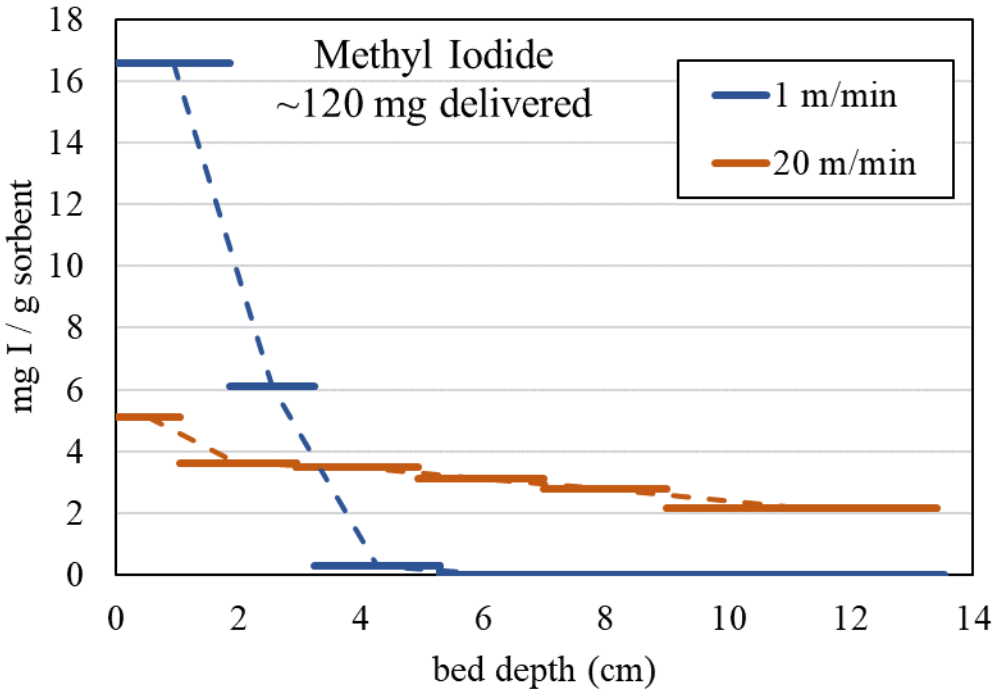

Figure 18. CH_3I penetration into a 14 cm AgZ bed at 1 m/min and 20 m/min superficial velocities. The experimental timescale was adjusted to normalize the mass of CH_3I delivered to the bed for both tests.

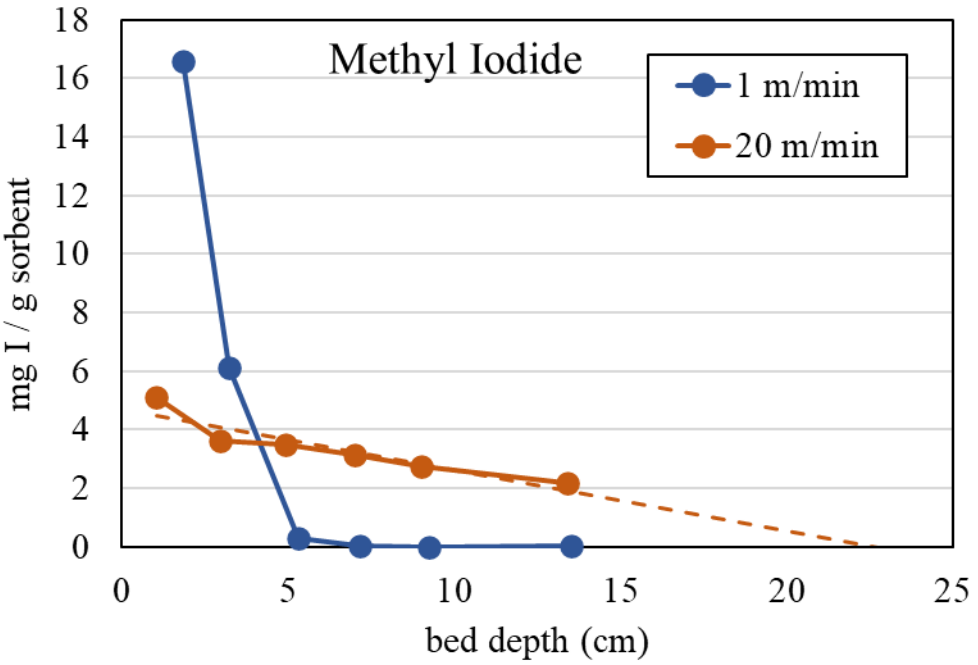

Figure 19. Estimated minimum penetration depth for 1 ppm CH_3I in a 20 m/min gas stream (orange dashed line).

3.3.4.2 Butyl Iodide

One 1 m/min test and two 20 m/min tests were completed to compare C_4H_9I loading on an AgZ bed as a function of the superficial velocity of the off-gas (Table 9). In test FVB-1-28, 11.9 mg of I were adsorbed to the 1 m/min bed. In test FVB-20-1, 7.5 mg of I were adsorbed to the 20 m/min bed over 32 h. In test FVB-20-28, 140 mg of I were adsorbed to the 20 m/min bed over 669 h.

Unlike the 1 ppm CH_3I tests, there was virtually no difference in bed penetration depth for the 20 m/min or 1 m/min tests when the experimental conditions were normalized to the mass of I delivered (e.g., when the 1 m/min test ran for 669 h and the 20 m/min test ran for 32 h) (Figure 20). In these C_4H_9I tests, 98% of the I was found in the first 7 cm (2.8 in) of the bed. Minor measurable I was observed on the outlet segment (segment F: 0.005–0.006 mg I/g sorbent). Although these mass loadings are low relative to the capacity of the sorbent, they indicate that micrograms of C_4H_9I can still pass deep into the bed in a short time period. Overall, these data indicate that the depth of I penetration into the bed is not affected by flow rate at parts-per-billion levels of C_4H_9I in the gas stream.

Additionally, data from the 20 m/min 28 day test (FVB-20-28) can be compared to the 1 m/min 28-day test (FVB-1-28) and to the 20 m/min 1 day test (FVB-20-1) The longer duration 20 m/min test delivered 140 mg of I to the sorbent bed, and 96% of that I was contained in the first 7 cm (2.8 in) (Figure 21), showing that it follows an S-shaped loading pattern similar to the 1 m/min test. However, over the 28 day time period, the depth of I penetration doubled between the 1 m/min test and the 20 m/min test from 5 to 10 cm (2 to 3.9 in.). Similarly, the I penetration depth doubled between the 1 day 20 m/min test and the 28 day 20 m/min test from ~5 to 10 cm (2 to 3.9 in.) (Figure 22). This suggests that the increase in I penetration depth in the 20 m/min 28 day test occurred because more I was introduced overall and is likely not a factor of flow velocity at low concentrations.

Overall, these data indicate that the increased superficial velocity of the VOG will likely affect the length and shape of the MTZ if there are elevated concentrations of organic iodides (~1 ppm) in the gas stream. In this concentration range, the VOG penetration depth could be two to three times longer than that expected in the DOG. However, if the VOG organic iodide concentration is lower (e.g., tens of parts per billion), then the gas velocity might not significantly impact the penetration depth or MTZ. The data at lower concentrations are inconclusive since saturation was not reached at the bed inlet.

Table 9. Results of C_4H_9I flow rate tests at 1 m/min (28 days), 20 m/min (1 day), and 20 m/min (28 days)

AgZ segment	Segment position	Segment mass (g)	Segment height (cm)	Total I (mg)	Concentration (mg I / g sorbent)	± 2σ (mg I / g sorbent)
1 m/min, 669 h (~28 days), 91 ppb C_4H_9I						
FVB-1-28-A	inlet	3.88	1.29	8.86	2.281	0.007
FVB-1-28-B		8.20	2.73	2.87	0.349	0.004
FVB-1-28-C		8.94	2.98	0.08	0.009	0.003
FVB-1-28-D		9.36	3.12	0.05	0.005	0.001
FVB-1-28-E		6.55	2.18	0.05	0.007	0.003
FVB-1-28-F	outlet	9.59	3.20	0.06	0.006	0.001
20 m/min, 32 h (~1 day), 59 ppb C_4H_9I						
FVB-20-1-A	inlet	6.18	2.06	5.71	0.924	0.096
FVB-20-1-B		6.71	2.24	1.56	0.232	0.025
FVB-20-1-C		6.78	2.26	0.15	0.022	0.002
FVB-20-1-D		8.90	2.97	0.04	0.004	0.001
FVB-20-1-E		7.34	2.45	0.01	0.001	0.001
FVB-20-1-F	outlet	10.4	3.47	0.05	0.005	0.001
20 m/min, 669 h (~28 days), 53 ppb C_4H_9I						
FVB-20-28-A	inlet	4.11	1.37	53.13	12.92	0.029
FVB-20-28-B		7.25	2.42	54.70	7.548	0.021
FVB-20-28-C		7.65	2.55	26.33	3.440	0.013
FVB-20-28-D		8.94	2.98	5.45	0.610	0.005
FVB-20-28-E		9.05	3.02	0.31	0.034	0.001
FVB-20-28-F	outlet	9.09	3.03	0.06	0.007	0.003

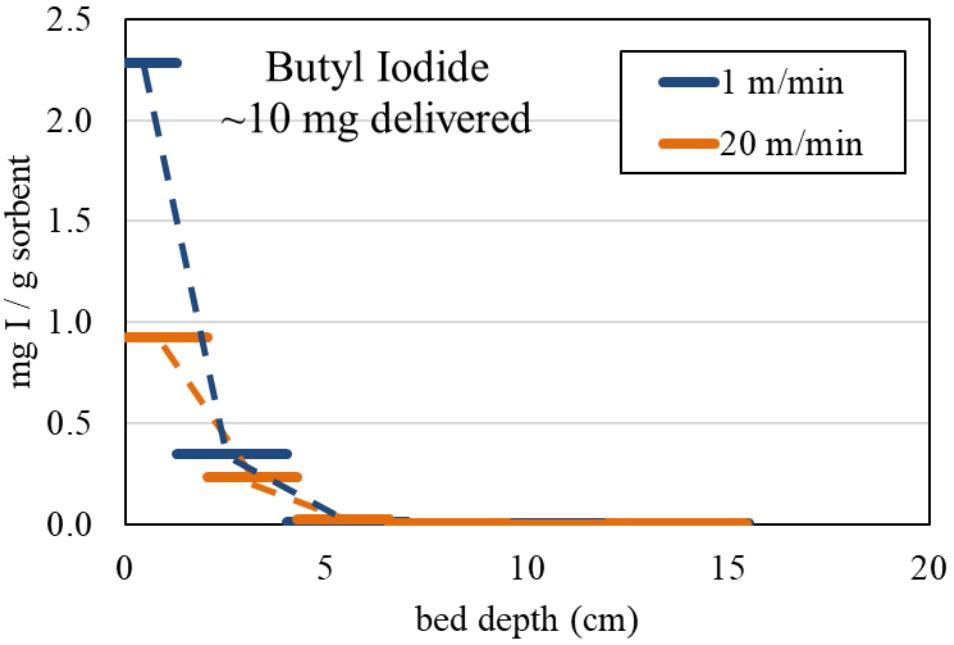

Figure 20. C_4H_9I penetration into a 15 cm AgZ bed at 1 m/min and 20 m/min superficial velocities. The experimental timescale was normalized to the mass of C_4H_9I delivered to the bed.

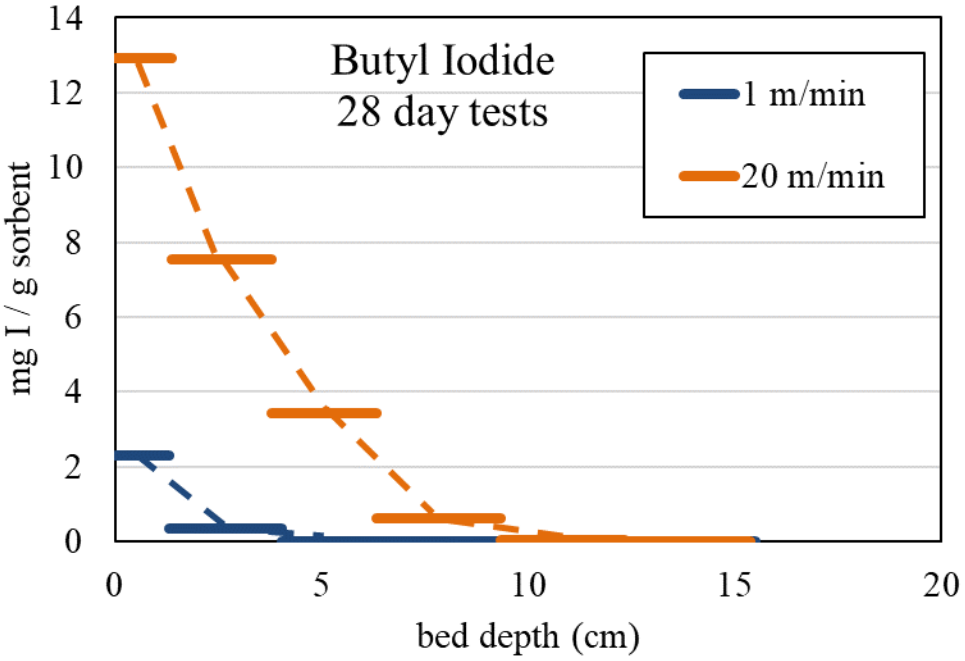

Figure 21. C_4H_9I penetration into a 15 cm AgZ bed at 1 m/min and 20 m/min superficial velocities, normalized to the duration of flow (669 h for both tests).

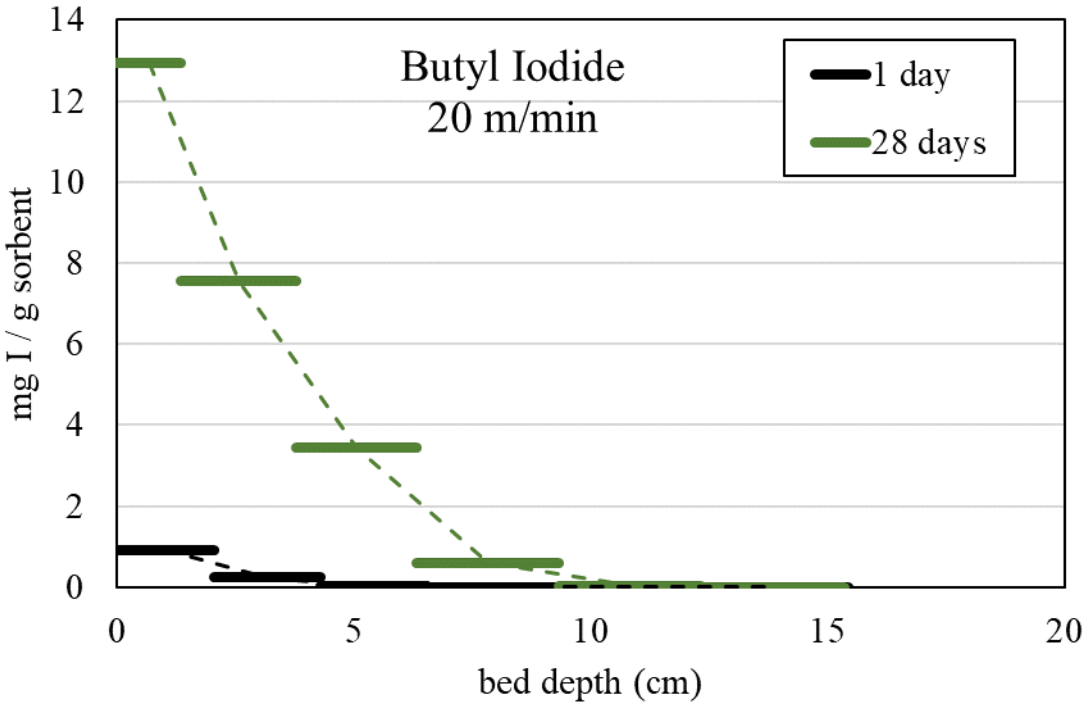

Figure 22. Shift in 20 m/min C_4H_9I loading curve between 1 day of loading and 28 days of loading.

3.3.5 Incomplete Organic Iodide Recovery from Deep Beds

The expected concentration of C_4H_9I in the gas stream was calculated to be ~1 ppm, but the C_4H_9I recovered from the sorbent bed translates to a gas phase concentration of 59–91 ppb. This mass balance discrepancy between gas and solid phase measurements has been a longstanding issue for deep-bed testing at low organic iodide concentrations (Jubin et al. 2017). Previous reports have considered and investigated the failure of the organic iodide volatilization method, leaks in the test system, low mass transfer to the sorbent (e.g. parts-per-billion- to parts-per-trillion-level organic iodide breakthrough), and physisorption of low concentration organic iodide to the sorbent that was removed as the bed was purged.

From these tests, it can be concluded that C_4H_9I is not breaking through the test bed at ppb-levels. This is because a second "excess" column of AgZ was used to catch the unused C_4H_9I that results from sequential dilution generated directly from the sparger. The concentration of the C_4H_9I flowing through this column should have been approximately 30 ppm, but the measured concentration of iodine sorption on this excess bed was low by the same factor as the 20 m/min and 1 m/min tests. Thus, an issue with butyl iodide generation resulted in the lower-than-expected concentrations in the gas stream. For example, because such low flow rates are used to generate a low concentration gas stream, a small leak that is difficult to detect (e.g., <5 sccm) in the C_4H_9I sparger could result in a <50% decrease in I concentration of the final gas stream.

Alternatively, it is possible that the low vapor pressure of C_4H_9I might have resulted in the deposition of this phase along any tubing that was not heat-traced for temperature regulation. The vapor pressure of C_4H_9I (10.5 mm Hg at 25°C) is such that room temperature is optimal for generating gas-phase C_4H_9I at the concentration range of interest; therefore, approximately 4 ft of tubing were not temperature regulated for these tests. To determine whether C_4H_9I/I was depositing along the portions of the tubing that was not heat traced, two PFA tubing pieces ¼ in. long were analyzed by NAA for I concentration. One piece of

PFA tubing was cut from the line ~12 in. downstream of the C_4H_9I sparger; this tubing was typically exposed to ~10 sccm of N saturated with C_4H_9I. A second piece of tubing was cut from the PFA line that contained the diluted gas stream before the entrance to the heat exchanger section in the oven ("to AgZ in oven" in Figure 7). The tubing near the sparger contained 0.09 wt % I, and the tubing at the oven entrance contained 0.0001 wt% I. If these values are extrapolated across the 4 ft of thermally unregulated tubing with the assumption that 1 ft of tubing contains 0.09 wt % I and 3 ft of tubing contains 0.0001 wt% I, then approximately 11.9 mg of I are expected to have deposited in the PFA tubing during C_4H_9I flow-rate testing. If this mass is evenly divided between the two flow-rate tests, this accounts for only ~5% of the C_4H_9I mass balance for each test and cannot fully explain the low C_4H_9I loadings.

3.3.6 Understanding Sorption Pathways

The goal of these experiments was to determine whether similar reaction pathways govern both CH_3I and C_4H_9I sorption onto AgZ. CH_3OH was detected as a reaction product of CH_3I sorption onto AgZ in the presence of water (Chebbi et al. 2016). Therefore, the working hypothesis that the sorption of C_4H_9I by AgZ will result in the formation of C_4H_9OH. A detailed literature review and preliminary experimental work is documented in Greaney and Bruffey (2021).

3.3.6.1 Effluent Testing

A series of tests were performed to test the primary hypothesis with the aim of detecting C_4H_9OH downstream of the AgZ bed. Test conditions varied the bed depth, gas stream humidity, and bed temperature post sorption (Table 10). The AgZ bed was contained within a 1 in. diameter column. The effluent gas stream downstream of the AgZ bed was sampled for GC-MS analysis.

Table 10. Test matrix of experiments completed with the goal of detecting organic iodide reaction products in the effluent.

SM test number	Species	Inlet conc. (ppm)	Sorbent	Temp. (°C)	Dew point (°C)	Carrier gas	Bed height (in.)	Bed mass (g)
FY21-SM-2	C_4H_9I	20	Ag^0Z	150	-65	Air	2	45
FY21-SM-3	C_4H_9I	20	Ag^0Z	150	10	Air	2	45
FY21-SM-4	C_4H_9I	50	Ag^0Z	150	-65	Air	1	18
FY21-SM-5	C_4H_9I	50	Ag^0Z	150	0	Air	1	18
FY21-SM-6	C_4H_9I	50	Ag^0Z	150	0	Air	0.25	4
FY21-SM-7	C_4H_9OH	50	Ag^0Z	150	-65	Air	0.25	4
FY21-SM-8	CH_3I	50	Ag^0Z	150	10	Air	0.3	6
FY21-013	C_4H_9OH	50	Ag^0Z	150	-65	Air	TGA test	2

Thin-bed C_4H_9I tests conducted at -65 and 0°C dew points did not result in C_4H_9OH detection in the effluent. The lack of C_4H_9OH detection could be due to one of four explanations. First, an insufficient mass of sorbent might have been used. If too few reaction sites were available for sorption, then detectable C_4H_9OH might not have been generated. Attempts were made to lower the detection limit of the GC analysis by using SPME fibers, but carryover between samples was too great, and the SPME fibers remained unacceptably contaminated for the repeated analysis of multiple experiments.

Another potential explanation is that at a dew point of -65°C (4 ppm H_2O) and 0°C (~3,600 ppm H_2O), not enough water is present in the system to promote a reaction pathway that results in C_4H_9OH formation. The previous detection of CH_3OH as a reaction product of CH_3I sorption occurred in experiments with a significantly higher water content in the gas stream (1.8% or 18,000 ppm) (Nenoff et al. 2014). Thin-bed CH_3I tests conducted at ORNL at a 10°C dew point resulted in the identification of CH_3OH in the chromatograph at levels near the LOD, tentatively confirming literature observations and the experimental methodology used in these studies. Further C_4H_9I deep-bed testing using deeper sorbent beds and an elevated dew point were planned, but maintenance issues with the GC-MS prevented effluent sampling for GC analysis.

A third possible explanation for the lack of C_4H_9OH detection in the sorbent bed effluent is that C_4H_9OH forms during the reaction but then physiosorbs to the sorbent bed. To test this hypothesis, two tests were conducted. The first test loaded C_4H_9I (SM-6) and C_4H_9OH (SM-7) on two AgZ beds simultaneously at 150°C before raising the temperature of the beds to burn off any physiosorbed reaction products. The temperature was increased incrementally by 25°C to 225°C, and no C_4H_9OH or C_4H_9I was observed in the effluent at elevated temperatures. The second test loaded a 50 ppm C_4H_9OH stream (diluted into air) onto a thin bed of AgZ in a TGA, recording any mass gain that occurred. This test ran for 1 week, and no mass gain was observed, implying that C_4H_9OH does not physiosorb to AgZ. These tests confirmed that if C_4H_9OH forms as a reaction product, it does not physiosorb to the sorbent during loading, and this hypothesis can be eliminated. This result is consistent with results reported by INL which also concluded that under the test conditions, no organic reaction byproducts could be detected on the sorbents after organic iodide sorption tests. INL occasionally detected a variety of organic compounds, including many that were not present in sufficient concentrations to be identifiable by GCMS, in the sorbent bed outlet. These partially oxygenated and/or nitrated compounds are reasonable byproducts of catalyzed separation of I from the organic moiety during I chemisorption. The partitioning of organic byproducts between alcohols; other oxygenated compounds, such as ketones and aldehydes; and nitrated compounds can reasonably depend on the presence of varied concentrations of water and NOx in those tests.

Consistent with the INL test results, these ORNL test results did not detect organic byproduct compounds in sufficient concentrations to show that a single or several organic compounds were produced that quantitatively represent the amount of the organic moiety in the original amount of the organic iodide. Because no significant amounts of organic compounds were detected as sorbed on the sorbent, perhaps other C and H gas species (e.g., CO, CO_2, H_2O) are more likely byproducts of the I chemisorption reactions, as indicated in Table 2.

Finally, C_4H_9I sorption to AgZ and accompanying reactions that occur in the gas phase might follow a different mechanism than CH_3I sorption.

3.3.6.2 SEM Imaging of AgZ

SEM imaging was used to determine whether there were differences in I loading patterns on AgZ between the various organic iodides. Four samples of I-saturated AgZ were analyzed: I-loaded AgZ, CH_3I-exposed AgZ, C_4H_9I-exposed AgZ, and $C_{12}H_{25}I$-exposed AgZ. SE and BSE images were collected on AgZ pellet cross sections, and elemental maps of Ag, I, Si, O, Al, and K were created via EDS. SE images show surface topography, and BSE images show variations in elemental mass distribution. Brightness indicates heavier elements that have larger nuclei that deflect electrons.

All analyzed AgZ pellets show similar morphological and chemical patterns, regardless of the form of I to which they were exposed. In SE imaging, rims are observed around the edge of the pellets that

appear smoother than the pellet core. This effect is observed in the *A/B*-axis and *C*-axis cross section in all pellets analyzed (Figure 23). Elemental EDS maps of the *A/B*-axis cross section of one pellet from each of the four samples are shown in Figure 24, Figure 25, Figure 26, and Figure 27. These maps do not show significant variations in chemical composition across the pellet. Notably, Ag and I are homogeneously distributed across all AgZ pellets along the *A/B*- and *C*-axes. Ag aggregates are observed in all AgZ pellets as "hot spots" on the Ag maps with accompanying I. These aggregates are approximately 5 µm in diameter and are thought to form during AgZ reduction.

The rims observed on the SE images do not represent the reaction front of I absorption on to the AgZ. These pellets had reached apparent I saturation on the TGA, which is confirmed by the homogeneous I distribution across *A*- and *C*-axis of the pellets. Additionally, the rims are observed in unmounted pellets, so they are not an artifact of mounting or polishing. The smoothed rims are hypothesized to form either as a result of oxidation and aging of the AgZ pellet as it is exposed to air or as a result of minor sintering of the mordenite as it is heated during reduction or testing. There are no differences in O concentration across the diameter of the pellet (Figure 24, Figure 25, Figure 26, and Figure 27), so these rims likely do not represent the formation of an oxidized silver species, such as Ag_2O. Because the rims appear to be a morphological boundary and not a chemical boundary, they likely represent minor sintering of the AgZ pellet. This proposed sintering effect does not affect I sorption.

In combination with visual observations of I distribution through the AgZ pellet on unsaturated samples, these SEM data suggest that I morphology within AgZ does not vary as a function of organic iodide speciation. Although the reaction products that form can vary by species, once I is cleaved from the chain, the sorption to and movement through the sorbent follow the same behavior.

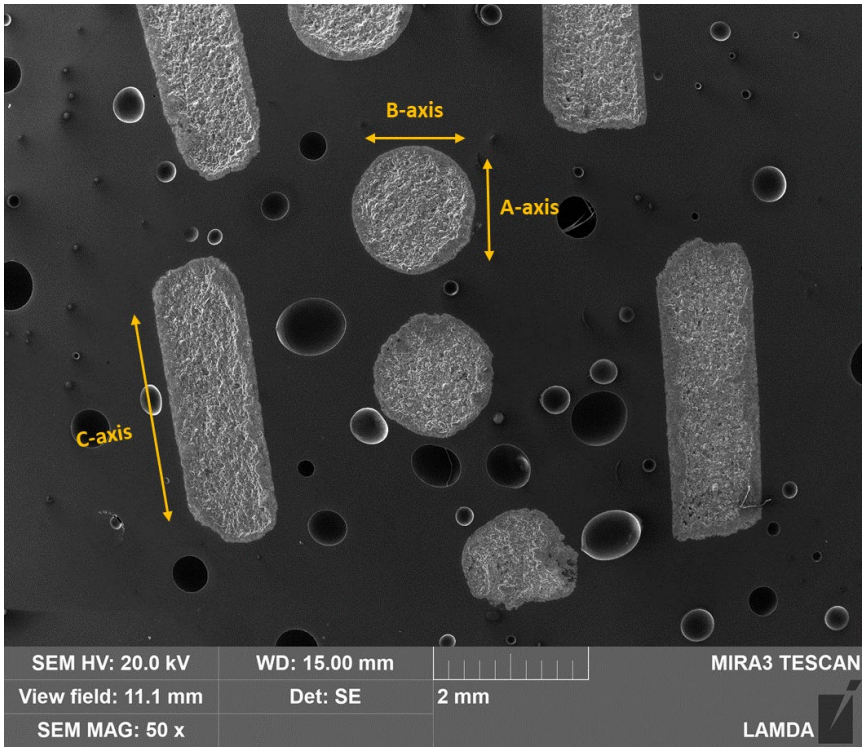

Figure 23. SE image of AgZ pellets loaded with butyl iodide that show the rim formed around the edge of each pellet.

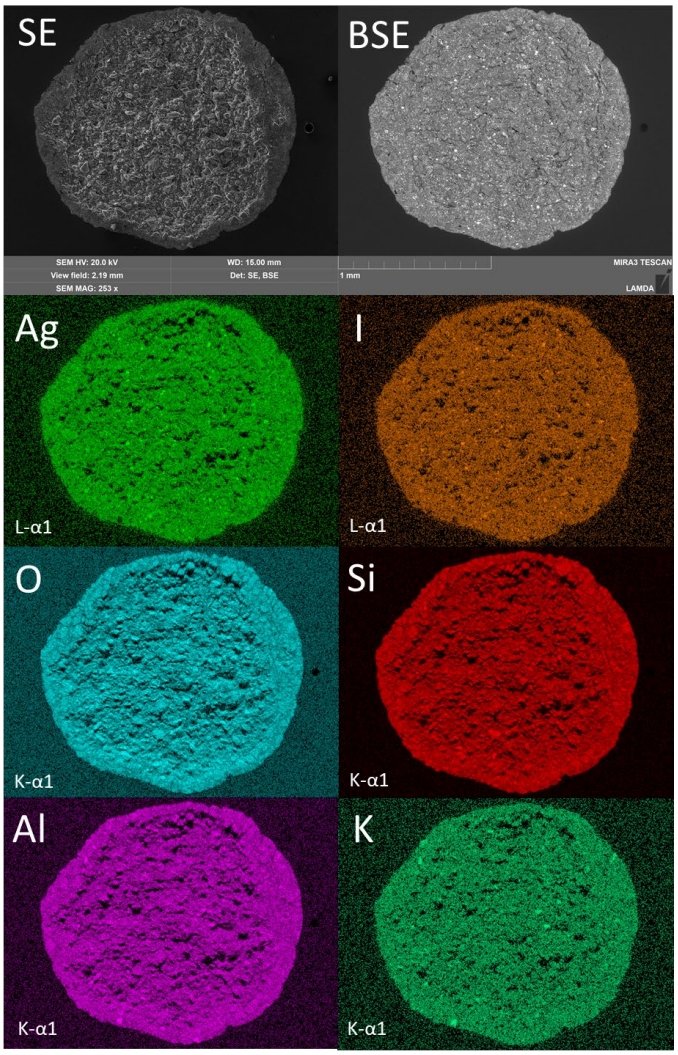

Figure 24. EDS elemental maps of an AgZ pellet cross section saturated in an I_2 gas stream. Pellet width is ~1.5 mm.

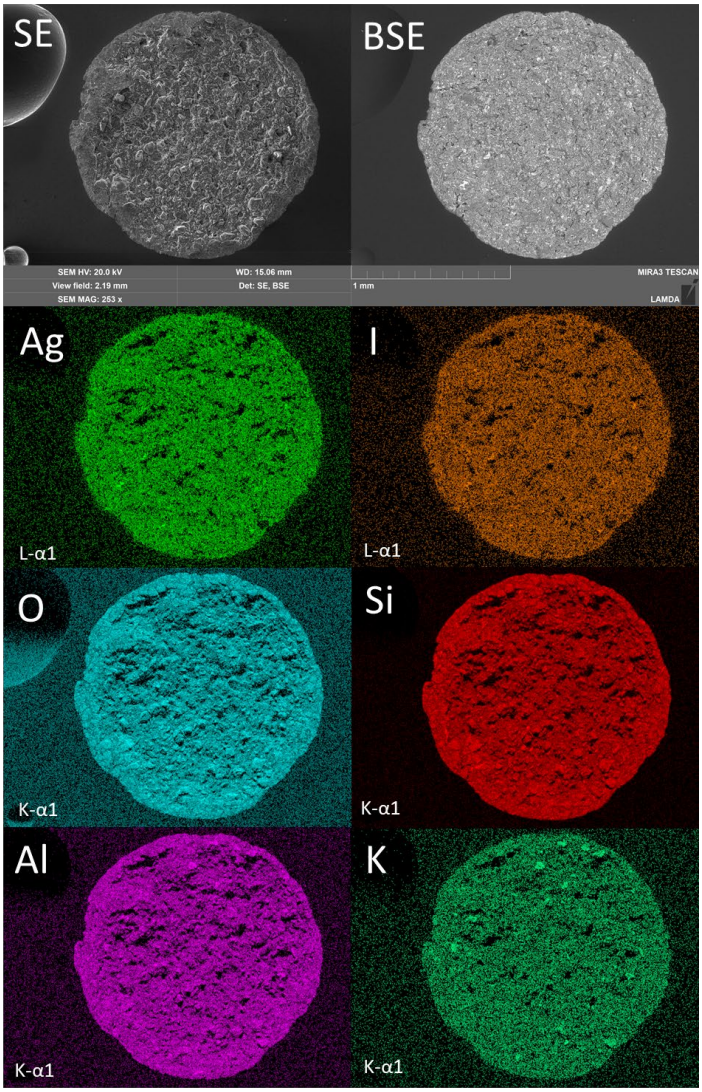

Figure 25. EDS elemental maps of an AgZ pellet cross section saturated in a CH_3I gas stream. Pellet width is ~1.5 mm.

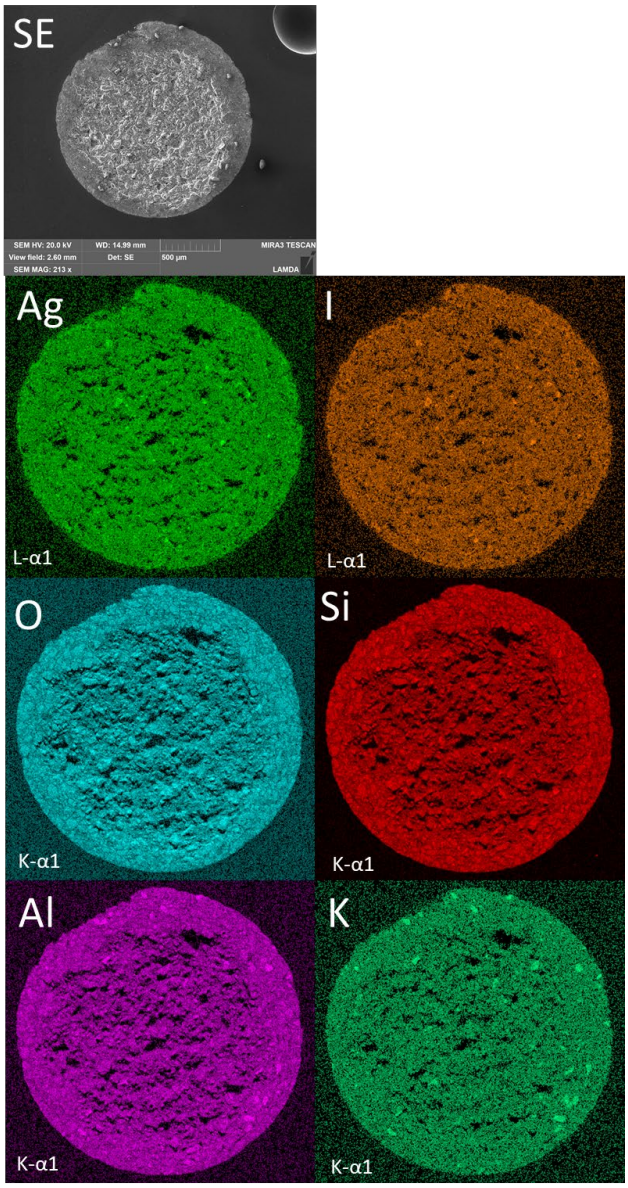

Figure 26. EDS elemental maps of an AgZ pellet cross section saturated in a C_4H_9I gas stream. Pellet width is ~1.5 mm.

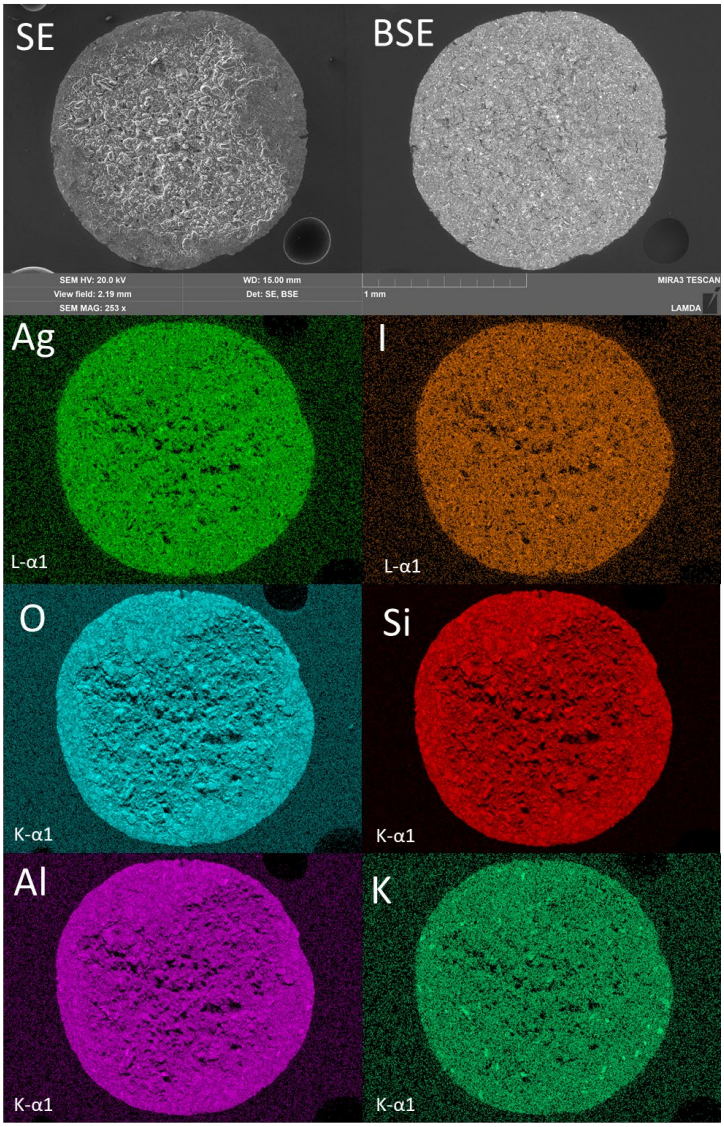

Figure 27. EDS elemental maps of an AgZ pellet cross section saturated in a $C_{12}H_{25}I$ gas stream. Pellet width is ~1.5 mm. Note the SE and BSE images are rotated 90° from the EDS maps.

3.3.7 Effects of Aging on Organic Iodide Sorption

To determine whether aging of the AgZ sorbent could have any sorbate species-dependent effects, the saturation capacity of 9 month aged AgZ was determined for each of the three organic iodides. (Table 11). Because of limited TGA availability, the CH_3I and C_4H_9I tests were completed in a 1 in. wide column in an oven by using a 50 ppm gas stream. These tests ran for 239 hours. The 25 ppm $C_{12}H_{25}I$ test was completed in the TGA over 260 hours, and the loading curve is presented in Figure 28. In the aged sorbent tests, issues with $C_{12}H_{25}I$ generation resulted in an initial spike in loading (Figure 28). A visual inspection of the AgZ pellets shows that the sorbent exposed to CH_3I reached apparent sorbent saturation (e.g., no core remained), whereas the C_4H_9I and $C_{12}H_{25}I$ tests did not saturate the AgZ pellet (e.g., an unreacted core remained). These data are consistent with loading rates calculated during previous thin-bed testing that show that C_4H_9I loads are ~15% slower and $C_{12}H_{25}I$ loads are ~35% slower than CH_3I at parts-per-million-level concentrations.

During CH_3I loading, the aged sorbent reached 71 mg I/g sorbent, which is approximately 66% the capacity of the fresh sorbent. During C_4H_9I loading, the aged sorbent reached 56 mg I/g sorbent, which is approximately 50% the capacity of the fresh sorbent. During $C_{12}H_{25}I$ loading, the aged sorbent reached 67 mg I/g sorbent, which is approximately 60% the capacity of the fresh sorbent. Thus, at high concentrations (25–50 ppm) of $C_{12}H_{25}I$ and C_4H_9I in the gas stream, aging the sorbent for 9 months decreased capacity from 35 to 50%. The C_4H_9I and $C_{12}H_{25}I$ aged sorbent capacity may be considered a conservative estimate because sorbent saturation might not have been achieved during the aged test.

Aging the sorbent not only decreases the sorbent capacity but also decreases the loading rate of organic iodides. Although loading curves are unavailable for the CH_3I and C_4H_9I tests, the time to sorbent saturation can be compared (Figure 29). The loading rates for the aged sorbent compared with fresh sorbent are presented in Table 11. Specifically, fresh C_4H_9I sorbent reached saturation within 187 h in a ~50 ppm stream (Table 7), whereas sorbent that had been aged 9 months only reached 50% of the fresh sorbent capacity in 239 h. On average across the organic iodides, the loading rate decreased by ~50% between fresh sorbent and nine-month aged sorbent. The $C_{12}H_{25}I$ rate comparison is not exact because the fresh sorbent test was exposed to a 50 ppm stream, whereas the aged sorbent test was exposed to a 25 ppm stream.

Previously reported data on I loading of aged AgZ show that adsorption capacity decreases over the first 4 to 6 months, but does not decrease further beyond that (Greaney and Bruffey, 2020). Thus, after 6 months, AgZ is not expected to continue to lose I capacity.

Table 11. Results of organic iodide testing on 9 month aged sorbent compared with fresh sorbent. The asterisks denote a comparison between a 25 and 50 ppm loading rate.

Parameter	CH_3I	C_4H_9I	$C_{12}H_{25}I$
Test duration (h)	239	239	268
Concentration (ppm)	50	50	25
Aged capacity (mg I/ g sorbent)	70.9	54.2	67
Fresh capacity (mg I/g sorbent)	107	111	112
Capacity decrease (%)	34	51	40
Aged loading rate (mg I/ g sorbent/h)	0.30	0.23	0.25
Fresh loading rate (mg I/ g sorbent/h)	0.64	0.56	0.42*
Rate decrease (%)	46	40	60*
Did aged sorbent reach apparent saturation?	Y	N	N

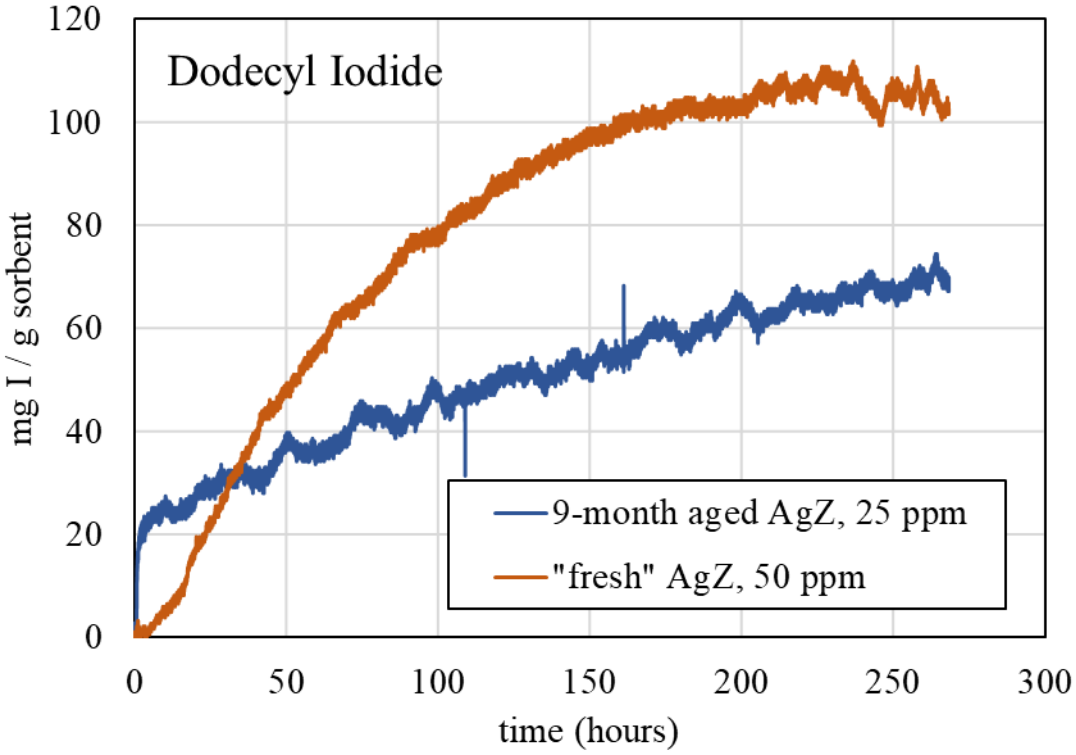

Figure 28. Loading curve of $C_{12}H_{25}I$ on aged AgZ (25 ppm) and fresh sorbent (50 ppm)

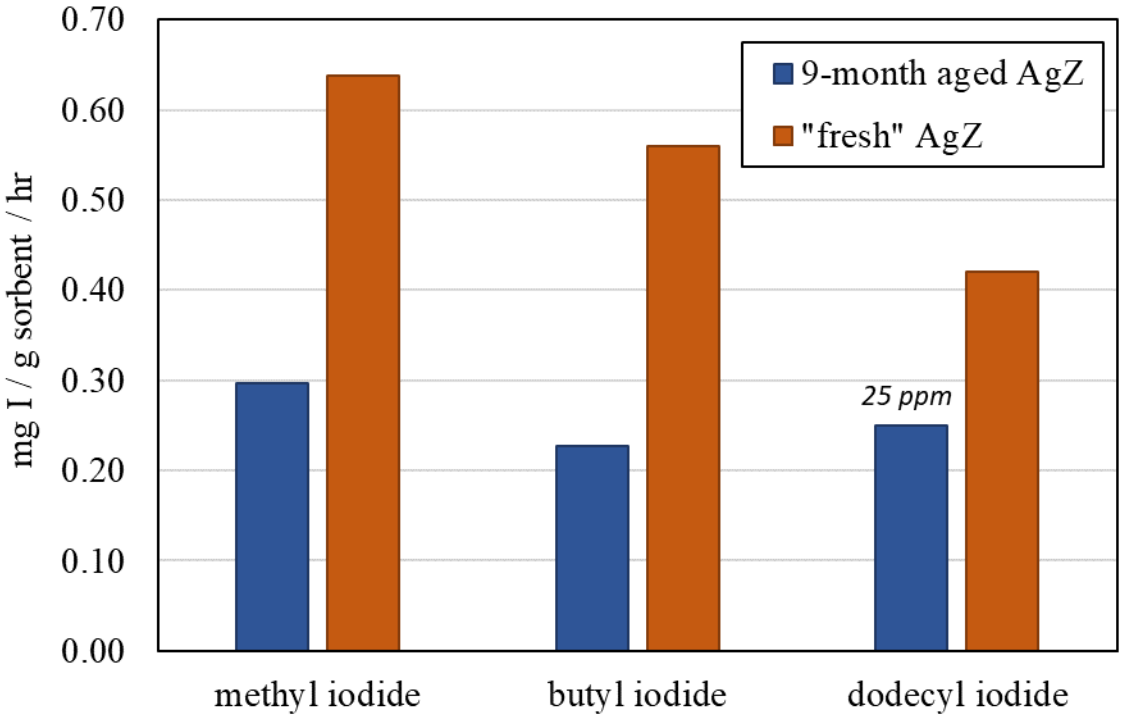

Figure 29. Comparison of the loading rate of 50 ppm organic iodide on fresh AgZ vs. AgZ that had been exposed to a humid air stream for 9 months.

3.4 SUMMARY OF ORNL 2021 RESULTS

Overall, the results of FY21 testing at ORNL can be initially summarized as follows.

- At ppm-level concentrations, I speciation does not affect sorbent capacity. At 50 ppm gas-phase sorbate concentration, all four species tested demonstrated AgZ saturation capacities of ~110 mg I/g sorbent.

- I speciation affects loading rate. AgZ saturation rate decreases as the C chain length of the sorbate increases.

- I gas-phase concentration affects loading rate. An order of magnitude decrease in organic iodide concentration in the gas stream results in at least a 60% reduction in overall loading rate.

- $C_{12}H_{25}I$ and C_4H_9I sorption follow a shrinking core sorption model. At saturation, I is distributed evenly across the pellet for all organic iodide species.

- Increased superficial velocity will affect the length and shape of the MTZ if there are elevated concentrations of organic iodides (~1 ppm) in the gas stream.

- Nine-month aged sorbent showed a capacity decrease of ~35% for CH_3I, ~50% for C_4H_9I, and ~40% for $C_{12}H_{25}I$. Thus, aging reduces capacity, but ~50–70 mg I/g sorbent loading is still achievable under parts-per-million-level concentrations of organic iodides in the off-gas stream. Additionally, 9 month aged sorbent loads organic iodides at approximately 50% the rate of fresh sorbent.

4. TOWARD A COMPREHENSIVE UNDERSTANDING OF ORGANIC IODIDE REMOVAL FROM DILUTE GAS STREAMS

In addition to previous findings from testing at ORNL and INL, the new and detailed data provided in this report can be used to develop a robust understanding of organic iodide behavior in dilute streams. This section provides additional details on previous work to support the key conclusions of this multiyear effort.

4.1 KEY FINDINGS OF COLLABORATIVE ORGANIC IODIDE TESTING PROGRAM (2017-2021)

Over the last four years, ORNL and INL have completed significant testing on the subject of organic iodide capture in the DOG and VOG. Key results are summarized here. These data are used in conjunction with data generated at ORNL in FY-2021 to answer the core questions posed in the Joint Test Plan (Jubin et al. 2018).

4.1.1 Organic Iodine Capture from Vessel Off-gas (INL)

Recently, INL published a report on organic iodiode capture from VOG streams in deep beds of AgZ (Soelberg et al. 2021). Two ~3,000 h tests were completed by using ~1 ppm streams of CH_3I and C_4H_9I. The feed gas streams also contained water (0°C dew point), and the sorbent beds were held at 150°C with a gas velocity of 10 m/min. The key results are summarized in Table 12. These tests show that under VOG conditions, AgZ capture of both C_4H_9I and CH_3I achieves DFs of >2,000 over a 2–5 month period. The MTZ ranged between 3 and 4.5 in. (7.6–11.4 cm) for both organic iodide species. After 3,774 h of C_4H_9I testing, the first 0.5 in. of the bed had reached saturation, and the last 2 in. of the bed recorded no I sorption. After 2,095 h of CH_3I testing, the first 1.5 in. of the bed had reached saturation, and the last

~1 in. recorded virtually no I sorption. No I breakthrough was observed downstream of the deep beds during these tests. One of the more interesting results of this testing is that even after 5 months of aging in a humid air stream, the capacity of the AgZ remained high at the inlet of the bed. This finding could drive off-gas equipment design toward smaller columns or the online addition of fresh sorbent to mitigate aging effects.

Table 12. Key results from INL deep bed organic iodide testing (data from Soelberg et al. 2021).

Parameter	Test 1	Test 2
Iodine species	CH_3I	C_4H_9I
Sorbent bed depth (in)	8.38	7.5
Concentration (ppm)	1.89	0.88
Test duration (months)	2.9	5.2
Max iodine loading (mg I/g sorbent)	130	137
DF	2000-9000	2000-3000
Penetration depth (in)	7.8	5.5
MTZ depth (in)	3 - 4.5	3.5 - 4.5

4.1.2 Comparison of Extended and Accelerated VOG Testing (ORNL)

ORNL completed two sets of experiments to understand the effects of aging on I and CH_3I sorption under VOG conditions (Table 13) (Greaney and Bruffey 2020). The first set of experiments compared sorbent capacity and MTZ length from ~200 ppb I and CH_3I loading in a humid air stream over 9 months. The second set compared sorbent capacity and MTZ length from CH_3I loading on to an AgZ deep bed over 28 days in an air vs. N gas stream. The aim of the second test was to determine whether sorbent aging effects by air had a measurable effect on capacity or penetration depth when compared with an inert gas stream.

The 200 ppb I_2 and CH_3I 9 month tests did not result in bed breakthrough. The maximum loading reached 47 mg I/g sorbent for the CH_3I stream and 57 mg I/g sorbent for the I_2 stream. Although these values are ~50% lower than the standard sorbent capacity, they may represent the maximum possible loading on 9 month aged sorbent, but this is speculative. Because it is unknown whether full sorbent capacity was reached at the bed inlet, an MTZ cannot be established. Instead, the penetration depth of the I can be evaluated; both I species penetrated 5 in. into the bed. This is slightly longer than the MTZs established by INL (3–4.5 in.) but shorter than the penetration depth observed by INL (7.8–5.5 in. for CH_3I and C_4H_9I, respectively) (Soelberg et al. 2021). If the inlet of the ORNL test bed is assumed to be saturated, then the ORNL MTZ is 5 in., which corresponds well to the data obtained at INL. If the inlet is not assumed to be saturated, then the ORNL MTZ will be >5 in., which is longer than that established at INL.

The potential difference in MTZ between 200 ppb ORNL testing and 1 ppm INL testing could be due to the lower concentration gas stream used and/or the difference in Ag content of the AgZ. The INL tests used an AgZ batch with >10 wt % Ag, whereas ORNL used AgZ with 9.4 wt % Ag (Soelberg et al. 2021). The lower Ag content on the ORNL AgZ will result in a lower overall sorbent capacity and ability for the I to penetrate deeper into the bed. Thin-bed tests show that lower concentration organic iodides are sorbed at relatively lower rates (Figure 13 and Figure 14). Thus, it is possible that the lower concentration iodide in the gas stream can penetrate deeper into the bed, resulting in a longer penetration depth and

ultimately a longer MTZ. Differences in test column ID at INL and ORNL—0.745 in. ID and 0.97 in. ID, respectively—could also contribute to MTZ disparity due to exaggerated edge effects on small-scale columns. MTZ measurements in low-concentration feed streams also heavily depend on the relative time when the measurements are made. The MTZ wavefront will continue to steepen with time until a stable pattern is developed. Where feed gas concentrations are extremely low, a stable wavefront takes longer to develop, exacerbated by sorbent aging. The likelihood of a test being terminated prior to before stable wavefront development is high, creating disparity among tests that are not identical.

The tests that compare N with air diluent streams did not show significant variations in loading behavior. Both tests resulted in similar sorbent capacities at the inlet of the bed (47 ± 1 mg I/g sorbent). The shape of the loading curve indicates that the inlet to the bed might have been saturated. Given the emission rates of the permeation tubes used to generate the CH_3I streams, both beds should have received the same amount of I, but the N test recovered 20% more I delivered than expected. This difference in total I loaded is likely a function of variations in permeation tube delivery than sorbent behavior under the different gas streams. Both sorbent beds recorded measurable I in the outlet AgZ segment at 6.3 in (16 cm). If the inlet is considered to have been saturated, then the MTZ for these tests is 5.3–6.3 in (13.4 to 16 cm). This MTZ is slightly longer than that established at INL, and the maximum sorbent loading is lower. The difference in maximum sorbent loading recorded by INL and ORNL tests could be explained by the analytical methods used. INL used SEM EDS to determine I concentration on the AgZ, which is calculated over a smaller sample size and/or pellet area than NAA data collected by ORNL, which averages a total across an entire bed segment. Overall, the air vs. N tests completed at ORNL show that oxidation by air over a 28 day period does not measurably impact AgZ capacity relative to using an inert diluent.

Table 13. Key results of deep bed tests performed at ORNL in 2020 (Greaney and Bruffey, 2020).

Parameter	Test 1a	Test 1b	Test 2a	Test 2b
I species	I_2	CH_3I	CH_3I	CH_3I
Sorbent bed depth (in.)	10.2	10.3	6.3	6.3
Gas composition	air	air	air	nitrogen
Test duration (months)	9	9	1	1
Total I loaded (g)	1.12	1.42	1.21	1.64
Mass balance to I generated (%)	120	110	102	120
Max I loading, averaged over one segment (mg I/g sorbent)	57	47	46	48
Penetration depth (in.)	4.9	5.0	6.3	6.3

4.1.3 Effects of NO_x and Water on I Sorption Rates (ORNL)

ORNL completed a series of experiments to test the effects of the DOG composition on AgZ capacity and loading rates of I and CH_3I (Greaney et al. 2020). Although the VOG is expected to contain most of the organic iodides evolved into the off-gas, minor organics present in the dissolver could result in the formation of CH_3I and possible C_4H_9I. Thus, these tests varied the NO_2%, NO%, dew point, and temperature of gas streams containing CH_3I and I_2 to simulate DOG conditions. The key findings are presented in Table 14. Overall, the presence of NO_2 and elevated temperature result in a statistically significant decrease in CH_3I and I_2 loading onto AgZ. This is likely due to oxidation of Ag on the sorbent.

Water and the presence of NO do not appear to affect the sorbent capacity. Specifically, the presence of 1% NO_2 in the DOG can decrease the capacity of AgZ up to 63% over week-long timescales. However, if NO_2 is balanced with NO, then the capacity only decreases by ~40%. These data can be used to refine design parameters in an engineering evaluation to ensure that any minor organic iodide formation in the DOG can be accounted for in abatement design.

Table 14. Effects of NOx, temperature, and water on CH_3I loading on AgZ (Greaney et al., 2020)

Temperature °C	NO (%)	NO_2 (%)	Dew point (°C)	Sorbent capacity (mg I/g sorbent)	Capacity change (%)
135	0	0	-70	90	baseline
165	0	0	0	101	+12
135	1	0	0	84	-7
165	1	0	-70	53	-42
135	0	1	0	33	-63
165	0	1	-70	37	-59
135	1	1	-70	75	-17
165	1	1	0	56	-38

Additionally, tests that compare the loading behavior of CH_3I and I_2 at elevated temperatures in the presence of NO_x suggest that NO_x could facilitate reactions in the gas stream to convert CH_3I to I_2. These observations are supported by Gibbs Free Energy (ΔG) calculations, which show that reactions between NO_x and organic iodides are thermodynamically favored to form inorganic I (Table 15). **Thus, in the presence of high NO_x concentrations, organic iodide sorption onto AgZ might not differ significantly from elemental I sorption.**

Table 15. Gibbs Free Energy (ΔG) calculations showing the effect of NO_x on converting organic iodides to iodine.

Organic iodide	Factor	Reaction	ΔG at 200°C (kJ/mol I)
CH_3I	NO_2	$14NO_2(g) + 8CH_3I(g) = 4I_2(g) + 12H_2O(g) + 8CO_2(g) + 7N_2(g)$	-855
CH_3I	NO	$14NO(g) + 4CH_3I(g) = 2I_2(g) + 6H_2O(g) + 4CO_2(g) + 7N_2(g)$	-1042
C_4H_9I	NO_2	$12.5NO_2(g) + 2C_4H_9I(g) = I_2(g) + 9H_2O(g) + 8CO_2(g) + 6.25N_2(g)$	-3010
C_4H_9I	NO	$25NO(g) + 2C_4H_9I(g) = I_2(g) + 9H_2O(g) + 8CO_2(g) + 12.5N_2(g)$	-3678

4.1.4 Retention of Organic Iodides on Silver-based Sorbents under DOG and VOG (ORNL & INL)

INL and ORNL issued a joint report in 2019 on thin-bed and deep-bed testing of C_4H_9I and CH_3I on AgZ and AgAero (Bruffey et al. 2019). These series of tests covered both DOG and VOG conditions and provided preliminary evidence for loading rate dependence on organic iodide chain length. In particular, C_4H_9I and CH_3I loading rates were calculated to be up to 50% slower than I loading rates. This is consistent with the more comprehensive data presented in this report that suggest that C_4H_9I and CH_3I adsorb onto AgZ 10–45% slower than I, depending on concentration.

These tests also established preliminary MTZs for CH_3I and C_4H_9I on AgZ and AgAero . INL found that for the two sorbents (AgZ and AgAero) and the two organic iodides (CH_3I and C_4H_9I) tested, the MTZ averaged 10 cm (3.9 in.). However, tests that simulated CH_3I in the DOG with the presence of NO_x resulted in MTZs up to 20 cm (7.8 in.). **Overall, these data are consistent with more recent reporting, suggesting that the MTZ could range between 3.5 and 6 in. for the VOG** (Soelberg et al. 2021, Greaney and Bruffey 2020).

This report also established DFs for CH_3I and C_4H_9I under a range of DOG and VOG conditions (Table 16). Deep-bed tests at INL showed that for almost all test conditions, DFs >2,000 could be established for CH_3I and C_4H_9I, which can support meeting I emission regulations. Two tests reported a DF <2,000. The first was a test with unreduced AgZ, which was expected because Ag reduction is key for I sorption to the sorbent. The other test simulated CH_3I sorption under DOG conditions with NO_x present, but this test was repeated, and a DF >10,000 was achieved.

Table 16. Range of DFs calculated during deep bed testing at INL (data from Bruffey et al. 2019)

Sorbent	I Species	Concentration (ppm)	Gas composition	DF
AgZ	I_2	1 – 50	DOG: NOx, H_2O	>10,000
AgZ	CH_3I	25 – 50	DOG: NOx, H_2O	5,000
AgZ (unreduced)	CH_3I	25	DOG: NOx, H_2O	1,000
AgZ	CH_3I	25	DOG: NO_x	1,000
AgZ	CH_3I	1 – 20	VOG: no H_2O	>10,000
AgZ	C_4H_9I	20	VOG: H_2O	2,000
AgAero	I_2	2 – 50	DOG: NOx, H_2O	>10,000
AgAero	CH_3I	40 – 60	DOG: NOx, H_2O	3,000
AgAero	C_4H_9I	1	VOG: no H_2O	>10,000
AgAero	C_4H_9I	25	DOG: NOx, H_2O	2,000

4.1.5 Performance of AgZ and Ag-Aerogel Under VOG Conditions (ORNL)

As referenced in Section 1, ORNL conducted a series of deep-bed tests by using low CH_3I and I concentrations (<1 ppm) to understand the effects of iodide concentration on sorption by AgZ and AgAero (Jubin et al. 2017). These tests resulted in incomplete mass balances and possible issues with CH_3I delivery to the column. However, these low-concentration data can be used to estimate the loading effects of parts-per-billion-level organic iodides onto AgZ and AgAero.

Importantly, these data show that the sorbent loading does not change significantly based on the target concentration in the gas stream; between 40, 400, and 1,000 pbb sorbent loadings varied between 24 and 30 mg I/g sorbent for AgAero and between 6 and 9 mg I/g sorbent for AgZ (Table 17). The total I loading on the sorbent was significantly lower than the capacity potential (maximum loading of 30 mg I/g sorbent), but these tests were generally terminated after ~10 days, so not enough I was delivered to reach sorbent capacity. The AgAero tests sorbed more I than the AgZ tests, but when the loadings were normalized to the Ag content of the sorbent, the Ag use was roughly equivalent. In concordance with more recent tests, the FY17 tests showed that AgZ is significantly more mechanically robust than the AgAero that produced significant fines during testing.

Table 17. Results of FY17 deep bed VOG CH_3I testing at ORNL (Jubin et al. 2017).

Parameter	Test 1	Test 2	Test 3	Test 4	Test 5	Test 6
Species	CH_3I	CH_3I	CH_3I	CH_3I	CH_3I	CH_3I
Sorbent	AgAero	AgAero	AgAero	AgZ	AgZ	AgZ
Sorbent bed depth (in)	3.5	3.5	3.5	4.3	4.3	4.3
Concentration (ppb)	40	400	1000	40	400	1000
Test duration (months)	0.5	0.3	0.1	3	0.3	0.3
Max I loading (mg I/g sorbent)	21	30	24	6.3	9.1	8.4
Mass balance to iodine generated (%)	50	114	80	39	34	50
Penetration depth (in)	2	1.6	1.6	1.6	1.4	2.4

4.2 JOINT TEST PLAN CORE QUESTIONS

The data generated at INL and ORNL over the last 4 years were used to answer the questions outlined within the joint test plan (Jubin et al. 2018) and are outlined in this section.

1) Is the sorption rate a function of organic iodide hydrocarbon chain length?

Yes, sorption rate is a function of organic iodide hydrocarbon chain length, and sorption rate decreases across the I, CH_3I, C_4H_9I, and $C_{12}H_{25}I$ series. Because longer chain organic iodides adsorb to AgZ more slowly than I, longer sorbent beds may be required in the VOG stream to effectively capture all I species. The macroscale parameter used in the sorbent bed design to account for sorption rate—which would also account for other parameters, including gas superficial velocity—is the MTZ.

2) Is the sorption rate a function of organic iodide concentration in the gas stream?

Yes, sorption rate is a function of organic iodide concentration in the gas stream. An order of magnitude reduction in gas-phase sorbate concentration resulted in a 60–75% decrease in loading rate. The lowest concentration loading rates calculated were in 5 ppm gas streams in which the AgZ sorbent gained, on average, 0.15 mg I/g sorbent per hour.

3) What is the saturation concentration of I for various organic iodides on AgZ, and does it vary with hydrocarbon chain length?

The saturation concentration does not vary with hydrocarbon chain length. ORNL thin-bed testing shows that at high concentrations in the off-gas stream (50 ppm iodide), the saturation concentration (110 ± 4 mg I/ g unaged sorbent) does not vary between CH_3I, C_4H_9I, and $C_{12}H_{25}I$ (Table 6). INL long-term deep-bed testing shows that at lower concentrations (1 ppm), the saturation concentration at the inlet to the deep bed (133 ± 4 mg I/g relatively unaged sorbent) does not vary between CH_3I and C_4H_9I (Soelberg et al. 2021). This 20 mg I/g sorbent difference in overall sorbent saturation between the two labs should be considered essentially equivalent, considering different test design and operating conditions—including different batches of AgZ and slightly varying sorbent reduction times—and analysis methods.

4) Does the ratio of physisorption to chemisorption vary with hydrocarbon chain length?

The simplest way to assess physisorption at ORNL is to use the TGA to measure the change in mass recorded as the I feed stream is cut off and dry air is used to purge the sorbent after loading has completed. With this method, no significant mass change is recorded during the purge period in dry tests (-70°C dew point), so physiosorption is not observed for any of the organic iodides (Figure 8). However, in one C_4H_9I test run in a humid atmosphere (0°C dew point), 15% mass loss was recorded during the purge period (Figure 13). This is likely due to dehydration of water and not organic iodide physiosorption. The INL tests have found the same result (minimal physiosorbed I) determined during post-test purging while sampling the effluent gas stream for I species; as long as the sorbent bed has not reached breakthrough.

5) How does gas velocity affect the sorption of organic iodides to AgZ?

Increasing the bed velocity will likely lengthen the penetration depth for sorption which may lead to an increased MTZ. One ppm methyl iodide tests at 20 m/min showed a broadened, linear loading profile relative to the exponential or S-shaped loading profiles for tests at 1 m/min and 10 m/min. In this concentration range, the VOG penetration depth is estimated at 22 cm long (8.7 in.) (minimum), which is up to three times longer than MTZs determined in 10 m/min tests (Soelberg et al., 2021) and is greater than four times longer than 1 m/min tests. However, if the sorbate concentration is lower (e.g., tens of ppb) the gas velocity may not have a significant impact on the penetration depth or MTZ, and MTZ similar to the DOG can be expected.

6) Do organic iodides follow similar sorption pathways onto AgZ?

The behavior of I sorption onto AgZ does not vary between organic iodide species. All organic iodides follow a shrinking core model of I sorption and diffusion into the sorbent pellet. At sorbent capacity, the distribution of I across the pellet is homogeneous between all organic iodide and I species. The iodide is cleaved from the hydrocarbon chain in the gas phase or on the sorbent surface, resulting in only I remaining on the sorbent (Soelberg et al. 2021). However, the reactions that result in the cleaving of the iodide at the sorbent interface or in the gas are still not fully understood for each organic iodide species.

7) What are the length and shape of the MTZ, and how do they vary or change for CH_3I and other organic iodides on Ag-based sorbents?

Extended deep-bed VOG testing completed at INL and ORNL calculate that the MTZ varies by 3–6 in. for AgZ. Tests conducted at 1 ppm CH_3I and C_4H_9I at INL established an MTZ between 3 and 4.5 in. over the course of 3–5 months. Tests conducted at 200 ppb I and CH_3I at ORNL estimate an MTZ of 5 in., but this might be a minimum because sorbent saturation might not have been reached at the inlet of the sorbent bed over the 9 month period. **Thus, sorbent beds exposed to lower concentration gas streams that are maintained for 9 or more months should account for a MTZ of up to 6 in in 10 m/min streams.**

Deep bed DOG tests were also conducted by INL using CH_3I and C_4H_9I (Bruffey et al. 2019). **These tests suggest that in the presence of NO_x, the MTZ for both organic iodides may extend to 7.9 in (20 cm).** These findings are consistent with reporting from ORNL showed the presence of NO_x may decrease sorbent capacity by up to 62% (Greaney et al., 2020).

The MTZ shape is similar for tests conducted at lower superficial velocities expected in the DOG (1 – 10 m/min). In these tests the initial penetration curve decreases exponentially within the first few centimeters of the bed.

8) What is the DF over a fixed length of bed as a function of concentration and I species in the feed gas?

Extended deep-bed testing at INL has established DFs of >2,000 for CH_3I and C_4H_9I (Soelberg et al. 2021, Bruffey et al. 2019) (Table 12 and Table 16). DF is unaffected by the concentration of the organic iodide in the gas stream over the range of 1 to 50 ppm until bed breakthrough occurs. Sorbent bed design and operation should consider the desired or practical bed replacement time, sorbent capacity, and desired number of multiples of the expected or bounding MTZ to avoid breakthrough, thereby ensuring adequate DFs during the bed operating life.

4.3 COMPARISON OF ORGANIC AND ELEMENTAL IODINE SORPTION BY AGZ

4.3.1 Nominal MTZ and DF for AgZ Sorbent Beds

Deep-bed testing shows that I and organic iodide sorption results in similar MTZ lengths. Extended VOG testing by INL in 2021 places CH_3I and C_4H_9I MTZs between 3 and 4.5 in. (7.6–11.4 cm) (Soelberg et al. 2021). Extended VOG testing by ORNL in 2020 placed CH_3I and I penetration depth at 5 in. (12.4 cm) and 4.9 in. (12.7 cm), respectively (Greaney and Bruffey 2020). The penetration depth of these tests can be considered an MTZ estimate, given assumptions presented in Section 4. VOG testing by ORNL in 2020 estimated the CH_3I MTZ at 6.3 in. (16 cm) (Greaney and Bruffey 2020). These data indicate that in low-concentration VOG conditions, organic iodides do not appear to penetrate deeper into the sorbent bed than inorganic I at 10 m/min. VOG MTZs range between 3.5 and 6.3 in. (7.6–16 cm) under varying conditions.

The only reported increase in penetration depth for organic iodides occurs in simulated DOG streams. Extended DOG testing by INL in 2019 placed the I and C_4H_9I MTZ at 3.9 in. (10 cm), C_4H_9I at 3.9 in. (10 cm), and CH_3I between 4.7 and 7.9 in. (12–20 cm). In this case, C_4H_9I recorded a similar MTZ as I, but CH_3I penetrated further into the AgZ bed. Thus, in 10 m/min DOG streams, MTZs for all iodide species range between 10 and 20 cm (3.9 to 7.9 in.).

All deep-bed tests show DFs >2,000 for I and organic iodides, except for one DOG test with NO_x present. Thus, if the VOG sorbent column is long enough to accommodate the migration of the MTZ over the sorbent bed lifetime, then regulatory DFs will be met for both I and the organic iodides.

4.3.2 Sorbent Capacity and Loading Rate

The I capacity of AgZ does not depend on I speciation in the gas stream. At DOG-level iodide concentrations (10–50 ppm), there is no difference between the sorbent capacity of AgZ when exposed to an I, CH_3I, C_4H_9I, or $C_{12}H_{25}I$ stream (Figure 8). At concentrations more realistic to the VOG between 1 and 5 ppm, there is not an obvious trend in variations in sorbent capacity for the various organic iodides vs. iodine.

However, loading rates vary as a function of I species. Longer chain iodides load more slowly than CH_3I and I. At concentrations expected in the DOG (e.g., 50 ppm), I adsorbs to AgZ the fastest (0.70 mg I/g sorbent per hour), and the organic iodides adsorb between 60 to 90% of that rate (0.42–0.66 mg I/g sorbent for $C_{12}H_{25}I$ and CH_3I, respectively) (Table 7). At concentrations more realistic of the VOG (5 ppm), I data are unavailable, but this trend is still expected to hold. At these concentrations, organic iodides load at an average rate of 0.14 mg I/g sorbent per hour.

4.3.3 Effects of Gas Stream Composition

Two systematic studies were performed comparing the effects of potential components in the gas stream on I and organic iodide sorption behavior. Greaney et al. (2020) compared sorbent saturation and loading rates of I and CH_3I sorption onto AgZ under variable concentrations of NO, NO_2, and water in the off-gas. The study found that these I species show similar loading patterns in the presence of these components, specifically that the presence of NO_2 significantly decreases AgZ capacity for both species. Additionally, the presence of NOx in the off-gas supports gas-phase reactions that convert organic iodides to iodine.

Bruffey et al. (2019) presents data on deep-bed studies of I, CH_3I, and C_4H_9I sorption under dry, humid, and NO_x-bearing gas streams at INL. Aerogel test data show that under high NO_x gas streams, sorbent capacity drops by ~45% from ~220 to ~120 mg I/g sorbent for C_4H_9I loading. Although the sorbent is different, this is a similar capacity decrease observed for CH_3I (between 40 and 63% decrease) and iodine (between 45 and 70% decrease) on AgZ exposed to NO_2. Although the sorbent capacity is expected to decrease when exposed to NO_x, particularly NO_2, these deep-bed tests show that AgZ beds exposed NO_x and humid gas streams can achieve a DF >10,000 for I, 1,000–5,000 for CH_3I, and 2,000 for C_4H_9I up until sorbent breakthrough.

4.3.4. Effects of Sorbent Aging

AgZ sorbent previously aged for 9 months in a humid air stream was tested for organic iodide capacity in 50 ppm gas streams. This 9 month aged sorbent showed a capacity decrease of ~35% for CH_3I, ~50% for C_4H_9I, and ~40% for $C_{12}H_{25}I$ (Table 11). Similar tests were completed for I loading on AgZ aged to different time intervals (Greaney et al. 2020, Bruffey et al. 2017). After 1 month of sorbent aging, capacity decreased by ~50%, and after 2 months, capacity decreased by ~60% and remains steady at that capacity up to 9 months of aging. Thus, four I species tested show a range of saturation concentrations on aged sorbent between 35 mg I/g sorbent (I) and 54 to 70 mg I/g sorbent (organic iodides).

During sorbent lifetime, the I capacity changes over the length of the sorbent bed. Fresh sorbent that is exposed to I immediately at the inlet of the bed will maintain a relatively high I capacity (>100 mg I/g sorbent), as evidenced by extended testing at INL (Soelberg et al. 2021). However, because the bed is continually exposed to humid air, the sorbent capacity near the bed outlet decreases to 35–70 mg I/g sorbent.

If the sorbent capacity decreases across the length of the bed during its lifetime and the mass of I migrating through the MTZ is held constant, then the MTZ must elongate to accommodate the same mass of I sorption onto lower-capacity sorbent. A conceptual model of this idea is illustrated in Figure 30. This model is not intended to quantitatively bound the change in MTZ length and is instead used to demonstrate the concept of MTZ migration and geometrical changes.

In this model, an AgZ sorbent bed that was 40 cm deep was assumed and divided into 10 segments of 4 cm each with an initial MTZ of 20 cm (7.9 in.), which is the maximum estimated for the DOG and minimum estimated for the VOG. The maximum sorbent capacity is 100 mg I/g sorbent. In the aged model, the minimum sorbent capacity on the most aged segment is assumed to be 35 mg I/g sorbent, and a linear decrease in sorbent capacity across the bed is assumed. The migration of the MTZ in a bed without aging effects is shown in the upper panel where the maximum possible sorbent capacity across the bed is 100 mg I/g sorbent (Figure 30). In this scenario, the MTZ maintains its shape and length as it migrates through the bed, always moving an equal mass of I through the MTZ.

However, if aging effects on the sorbent capacity are considered, then the MTZ geometry and length will change, as illustrated in the lower panel of Figure 30. Here, the maximum possible sorbent capacity

decreases across the length of the bed as the sorbent ages during I loading. Once again, the mass of I contained within the MTZ is held constant in this model. Because the mass of I moving through the MTZ is held constant, the MTZ must lengthen over time to accommodate the overall lower sorbent capacity deeper in the bed. In this conceptual model, the MTZ increases from 20 to 25 cm (7.9 to 9.8 in.) over four time periods.

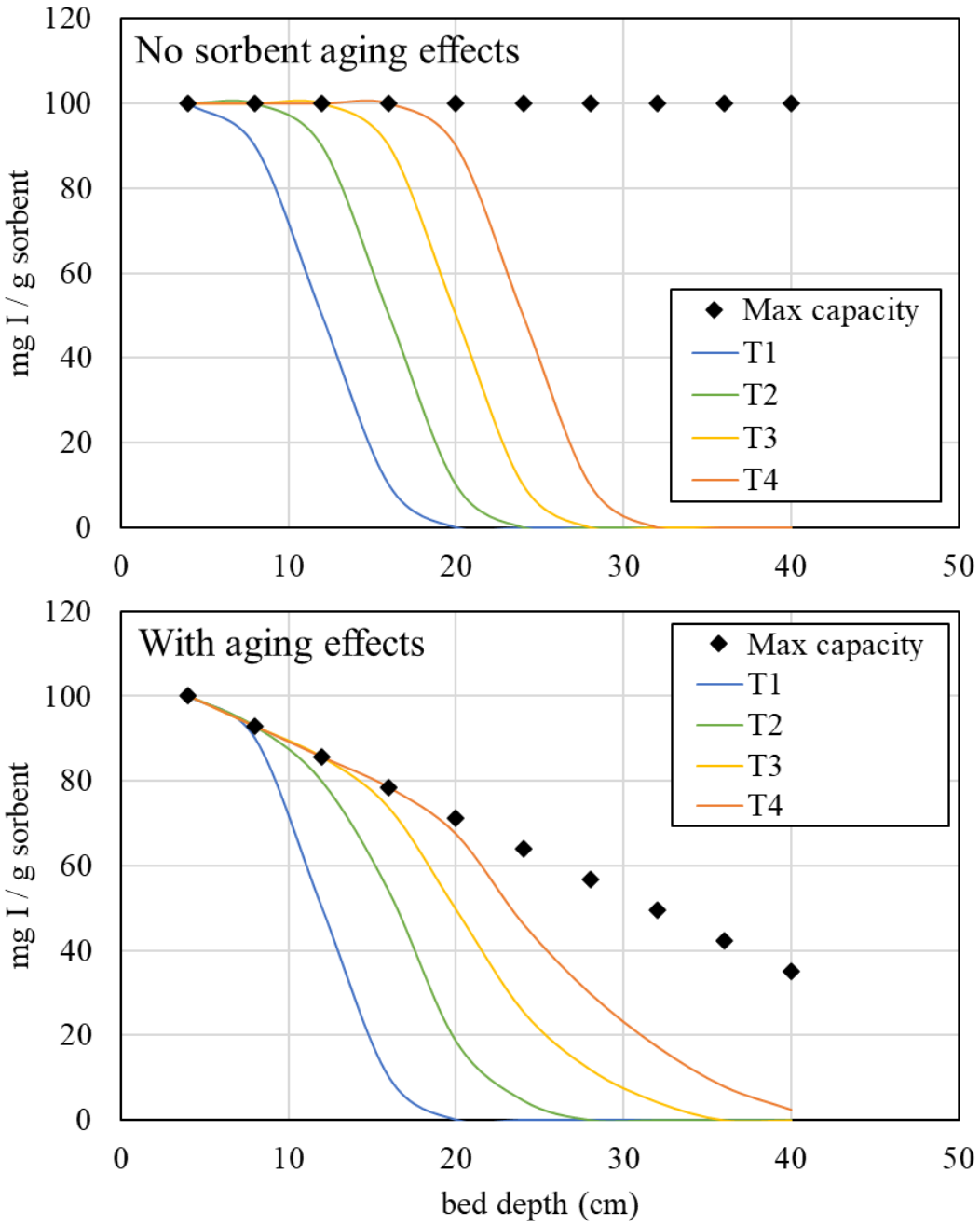

Figure 30. Conceptual model of MTZ migration in a sorbent bed with and without aging effects (e.g., decrease in sorbent capacity) at four time periods. The mass within the MTZ is kept constant between the unaged and aged sorbent models.

4.3.5 Variations Between AgAero and AgZ

Ag-functionalized aerogels created at PNNL are designed with higher Ag loadings on the sorbent relative to AgZ, and as such they routinely show a greater capacity for iodide sorption on a mass basis. The AgAero sorbent capacity and durability vary with experimental batches, so all data obtained thus far might not be representative of a final engineered version. Comparative experiments at ORNL of AgZ and AgAero under DOG conditions show that under dry gas streams, the FY20 AgAero can load more than 300 mg I/g sorbent compared with 100 mg I/g sorbent nominal loading on AgZ. Both sorbents show a significant capacity decrease when exposed to NO_x with the FY20 AgAero experiencing additional mechanical degradation.

INL completed deep-bed experiments for I, CH_3I, and C_4H_9I loading on the FY19 AgAero (Bruffey et al. 2019). These experiments show that DFs >10,000 can be achieved for parts-per-million-level I sorption, and DFs >2,000 can be achieved for parts-per-million-level C_4H_9I and $C_{12}H_{25}I$. Thus, like AgZ, deep beds of AgAero can produce the DFs needed for organic iodide sorption, however the mechanical stability of AgAero is lower than that of AgZ and would require a control mechanism for fines generated during use.

5. DESIGN OF A FULL-SCALE VOG ABATEMENT SYSTEM

The first attempt at a full-scale VOG iodine abatement system was described in Jubin, et al. (2016) and was designed to support iodine abatement within a 1000 MT/y nuclear fuel reprocessing facility. In the years following publication of that study, concerted effort was made to answer the questions posed, and fill the data gaps identified, by the evaluation team. Iodine capture and sequestration from VOG streams was noted as a significant data gap. While studies had been conducted at more concentrated dissolver off gas (DOG) iodine concentrations, little was known about the efficacy of existing capture technologies at the much lower concentrations in VOG. The wealth of data collected since then and described in this report allows a re-examination of that design and the assumptions that support it.

The difference between the assumptions made in 2016 and subsequent research results is significant enough to warrant an update to the VOG section of the 2016 engineering evaluation. The updated evaluation can be found in a supporting document entitled "*Updated Engineering Evaluation: Vessel Off-Gas Treatment System for Used Nuclear Fuel Reprocessing Facilities*" (Welty et al. 2021; INL-LTD-21-64587). Key results are summarized as follows.

The most impactful change since the 2016 engineering evaluation is the addition of replicable data indicating that the capacity of the silver mordenite sorbent is up to 10 times higher than was initially estimated. These findings allowed the VOG iodine capture system to decrease in both size and complexity. The design and operating scheme presented in the updated report represents the best option given the information available at this time. However, since this is not a detailed engineering design, there are a number of other options that should be considered during more detailed design discussions.

Columns are kept relatively short in order to minimize pressure drop. Additionally, it is considered advantageous to keep hot cell size minimized. However, this choice results in a relatively large percentage of the AgZ in each column with available capacity when the column banks are switched. Given the already lengthy operating time for these columns, it may not be wise to decrease the ratio of unused sorbent by simply increasing the column height. The end result of may be decrease bed life due to increased pressure drop.

A design and operating scheme like that recommended in 2016 could be employed. An additional bank of columns could be installed solely for the purpose of capturing iodine that breaks through the primary beds once the leading edge of the MTZ has reached the top of the beds. However, this would increase the system footprint by about 30%, which may not be feasible in a hot cell.

Using the current setup, once the MTZ leading edge has reached the top of the primary beds, flow from those beds could be routed into the next set of beds until the primary beds have reached complete saturation, utilizing the entire beds and reducing stored waste by approximately 35%. However, this scheme will cause premature aging of the second set of beds, reducing their capacity prematurely.

Rather than banks of five beds, larger banks of smaller-diameter columns could be used. This would have the advantage of decreasing the ratio of partially used sorbent material. This would add additional complication in a hot cell – more pipes, more valves, and more columns.

6. CONCLUSIONS

This study presents data that can be used for inorganic and organic iodide capture in off-gas that meets US EPA regulatory requirements. This was completed through three objectives: 1) present new data obtained by ORNL in 2021 on organic iodide sorption to AgZ, 2) summarize and synthesize data collected by ORNL and INL over the last few years to understand fundamental and applied characteristics of organic I sorption from dilute gas streams, and 3) apply these data to design an updated VOG iodine abatement system that reflects recent technological progress.

The experimental work completed at ORNL and INL produced some of the first published data on butyl iodide and dodecyl iodide sorption behavior. These include determining sorption rates for the three organic iodides and I on AgZ at various concentrations, total sorbent capacity and the effects of aging on sorbent capacity for organic iodides and I, and the length and shape of the I loading profile in a sorbent bed. Most importantly, these data show that **if the MTZ is accommodated in sorbent bed design for the DOG and VOG, regulatory requirements set by US EPA will be met.** Specific experimental findings are summarized below.

1. The sorption rate of organic iodides onto AgZ depends on the hydrocarbon chain length. Longer chain organic iodides adsorb to AgZ more slowly than I. For example, at a concentration of 50 ppm concentration in the off-gas, CH_3I loads 8% slower, C_4H_9I loads 20% slower, and $C_{12}H_{25}I$ loads 40% slower than I.

2. The sorption rate is a function of organic iodide concentration in the gas stream. An order of magnitude reduction in concentration resulted in a 60–75% decrease in loading rate. The lowest concentration loading rates calculated were in 5 ppm organic iodide gas streams in which AgZ gained 0.14 mg I/g sorbent per hour on average. Thus, longer sorbent beds might be needed to accommodate slower loading rates onto AgZ in lower concentration gas streams.

3. Although sorption rate varies as a function of hydrocarbon chain length, the saturation concentration of AgZ does not vary. ORNL thin-bed and INL long-term deep-bed testing show that at between 1 and 50 ppm, the saturation concentration at the inlet of an AgZ bed does not show clear differences between I, CH_3I, C_4H_9I, and $C_{12}H_{25}I$. AgZ unaged saturation capacity is ~100 mg I/g sorbent for all I species studied.

4. The MTZ length generally ranges between 3 and 6 in. (8–16 cm) for I and the organic iodides in 10 m/min DOG streams but could extend up to 7.9 in. (20 cm) if NO_x is present. DOG MTZs should be conservatively estimated at 7.9 in (20 cm) for a 10 m/min gas superficial velocity

5. Aging AgZ in a humid air stream for 9 months drops the overall capacity by ~35% for CH_3I, ~50% for C_4H_9I, and ~40% for $C_{12}H_{25}I$. This results in a saturation capacity between 35 and 70 mg I/g sorbent.

6. The VOG MTZ could be a different shape than in the DOG. A 20 m/min 1 ppm CH_3I test showed a nearly-linear loading profile with an extrapolated penetration depth of 22 cm (8.6 in). At the higher flow rates expected in the VOG, the iodide is more evenly distributed across the length of the sorbent bed relative to the lower flow rate tests. However, at lower concentrations (50–90 ppb), the 20 m/min loading profile takes on a shape similar to the 10 m/min tests with loading decreasing exponentially across the first few centimeters of the bed. If 1 ppm organic iodide concentrations are assumed in the VOG, then the sorbent bed should be designed to accommodate a longer MTZ.

7. Deep-bed testing at INL has established DFs of >2,000 for I, CH_3I, and C_4H_9I under a range of conditions (Soelberg et al. 2021, Bruffey et al. 2019). DF is not affected by the concentration of the organic iodide in the gas stream over the range of 1 to 50 ppm until bed breakthrough occurs. Thus, if the MTZ is accommodated in sorbent bed design for the DOG and VOG, regulatory DFs will be met.

These data are used to re-evaluate previous engineering designs for the VOG. The updated engineering evaluation can be found in the accompanying document entitled "*Updated Engineering Evaluation: Vessel Off-Gas Treatment System for Used Nuclear Fuel Reprocessing Facilities*" (Welty et al. 2021; INL-LTD-21-64587). This re-evaluated engineering design finds the VOG iodine capture will decrease in both size and complexity, relative to previous designs.

Completion of these three objectives not only provides an important reference for industry and others seeking to understand both fundamental and applied organic iodide behavior in an aqueous-based nuclear fuel reprocessing facility but also serves to demonstrate that the US possesses the technology needed to limit radioactive organic iodide emissions from aqueous-based nuclear fuel reprocessing facilities to levels that are safe for the general public and compliant with emissions regulations.

7. ACKNOWLEDGEMENTS

The authors thank Dr. Rachel Seibert at ORNL for conducting SEM analyses and David Glasgow at ORNL for conducting NAA measurements of loaded AgZ pellets.

8. REFERENCES

Ackley T.D. and Combs Z. (1973) Applicability of Inorganic Sorbents for Trapping Radioiodine from LMFBR Fuel Reprocessing Off-Gas. Report No. ORNL/TM-4227, Oak Ridge National Laboratory

Adams, RE, Ackley R.D., Browning W.E. (1967) Removal of Radioactive Methyl Iodide from Steam-Air Systems. Report No. ORNL-4040, Oak Ridge National Laboratory

Broothaerts, J, G Collard, A Bruggeman, WRA Goossens, LH Baetsle, and R Glibert (1976) Treatment and Control of Gaseous Effluents from Light Water Reactors and Reprocessing Plants. In Proceedings of the Management of Radioactive Wastes from the Nuclear Fuel Cycle, 101-14 pp. International Atomic Energy Agency

Billard F. (1967) Methods adopted in France for the removal of radioactive iodides. ORNL-tr-2504, Oak Ridge National Laboratory

Browning W.E. Jr. (1963) Removal of Radioiodine from Gases, *Nuclear Safety*, 6 (3), 272-79.

Bruffey S.H., Spencer B.B, Jubin R.T., Strachan D., Soelberg N., Riley B.J. (2015) A Literature Survey to Identify Potentially Problematic Volatile Iodine-bearing Species in Present in Off-gas Streams, ORNL-SPR-2015/290, Oak Ridge National Laboratory

Bruffey S.H., Jubin R.T., and Jordan J.A. (2016) Organic Iodine Adsorption by AgZ under Prototypical Vessel Off-Gas Condition, ORNL/TM-2016/568, Oak Ridge National Laboratory

Bruffey S.H., Jubin R.T., and Jordan J.A. (2017) Organic Iodine Adsorption by AgZ under Prototypical Vessel Off Gas Conditions. Report No. FCRD-MRWFD-2016-000357, Oak Ridge National Laboratory

Bruffey S.H., Greaney A.T., Jubin R.T., Soelberg N., and Welty A.K. (2019) Iodine Retention of Long Chain Organic Iodides on Silver Based Sorbents under DOG and VOG Conditions, ORNL/SPR-2019/1359, Oak Ridge National Laboratory

Chapman K.W., Sava D. F., Halder G. J., Chupas P. J. and Nenoff T. M. (2011) Trapping Guests within a Nanoporous Metal–Organic Framework through Pressure-Induced Amorphization, *Journal of the American Chemical Society*, 133, 18583–18585.

Chebbi M.B., Azambre L., Cantrel, and Koch A. (2016) "A Combined DRIFTS and DR-UV−Vis Spectroscopic In Situ Study on the Trapping of CH_3I by Silver-Exchanged Faujasite Zeolite," *Journal of Physical Chemistry C* 120: 18,694–18,706.

Dexter A.H., Evans A.G., and Jones L.R. (1977) Iodine Evaporation from Irradiated Aqueous Solutions Containing Thiosulfate Additive. In Proceedings of the Fourteenth ERDA Air Cleaning Conference, 224-32 pp. The Harvard Air Cleaning Laboratory, Cambridge, MA.

Environmental Protection Agency (EPA) (2010a) Chapter 40. Environmental Protection Agency: Part 61–National Emission Standards for Hazardous Air Pollutants. Subpart H—National Emission Standards for Emissions of Radionuclides Other Than Radon from Department of Energy Facilities, 92—Standard. 40 CFR 61.92. US Environmental Protection Agency, Washington, DC.

Environmental Protection Agency (EPA) (2010b) Protection of Environment: Chapter I–Environmental Protection Agency (Continued), Part 190 Environmental Radiation Protection Standards for Nuclear Power Operations. 40 CFR 190.10. US Environmental Protection Agency, Washington, DC.

Evans, GJ and RE Jervis. 1992. "Radiochemical Studies of Iodine Behavior under Conditions Relevant to Nuclear Reactor Accidents." *Journal of Radioanalytical and Nuclear Chemistry* 161(1):121-33. 10.1007/BF02034886.

Greaney A.T. and Bruffey S.H. (2020) Comparison of Extended and Accelerated VOG Tests, ORNL/SPR-2020/1544, Oak Ridge National Laboratory

Greaney A.T., Bruffey S.H., and Jubin R.T. (2020) Effect of NOx and Water Variations on Iodine Loading of AgZ, ORNL/SPR-2020/1581, Oak Ridge National Laboratory

Greaney A.T. and Bruffey S.H. (2021) Analysis of Organoiodide Adsorption Mechanisms, ORNL/SPR-2021/2003, Oak Ridge National Laboratory

Haefner, D. R., and Soelberg N. (2009) Experimental Sorption Testing of Elemental Iodine on Silver Mordenite, INL/EXT-09-16837

Jubin (1981) Organic iodine removal from simulated dissolver off-gas systems utilizing silver-exchanged mordenite, AIChE Meeting, New Orleans, LA

Jubin R.T. (1994) The mass transfer dynamics of gaseous methyl-iodide adsorption by silver-exchanged sodium mordenite, The University of Tennessee, Knoxville

Jubin, R.T, N.R. Soelberg, D.M. Strachan, and G. Ilas (2012) Fuel Age Impacts on Gaseous Fission Product Capture During Separations, FCRD-SWF-2012-000089

Jubin, R. T., Strachan D.M., Soelberg N.R., and Ilas G. (2013) Iodine Pathways and Off-Gas Stream Characteristics for Aqueous Reprocessing Plants—A Literature Survey and Assessment. Report No. FCRD-SWF-2013-000308, Oak Ridge National Laboratory, Oak Ridge, TN.

Jubin R.T., Bruffey S.H., Spencer B., (2015) Performance of silver-exchanged mordenite for iodine capture under Vessel Off-gas Conditions, *Proceedings of Global 2015*

Jubin R.T., Jordan J.A., Spencer B., Soelberg N.R., Welty A.K., Greenhalgh M., Strachan D.M., Thallapally P.K. (2016) Engineering Evaluation of an Integrated Off-Gas Treatment System for Used Nuclear Fuel Reprocessing Facilities, FCRD-MRWFD-2016-000313, INL/LTD-16-39698, ORNL/TM-2016-447

Jubin, R. T., Jordan J.A., and Bruffey S. H. (2017) Performance of Silver-Exchanged Mordenite and Silver-Functionalized Silica-Aerogel Under Vessel Off-gas Conditions. Report No. NTRD-MRWFD2017-000034, Oak Ridge National Laboratory

Jubin R.T., Bruffey S.H., Soelberg N.R., Welty A.K. (2018) Joint test plan to for the evaluation of iodine retention for long-chain organic iodides, NTRD-MRWFD-2018-000212

Li J.C.M. and Rossini F.D. (1960) Vapor Pressures and Boiling Points of the 1 -Fluoroalkanes, 1 -Chloroalkanes, 1-Bromoalkanes, and 1-lodoalkanes, C to C20, *Journal of Chemical and Engineering Data*, 268-270

Matyáš J., Kroll G., and Li X.S. (2018) Improvement of mechanical stability of Ag0 -functionalized silica aerogel, FCRD-MRWFD-2018-000214, Pacific Northwest National Laboratory, Richland

Matyáš J., Kroll G., and Li. X.S. (2019) Mechanically Stable Silver-Functionalized Silica Aerogel, PNNL [1] 29048. Pacific Northwest National Laboratory, Richland, WA

Matyáš J., Sannoh S.E., and Li. X. (2020) Development of a Robust Ag0 -Functionalized Silica Aerogel for Capturing Iodine Gas, PNNL-30732. Pacific Northwest National Laboratory, Richland, WA

Matyáš J., Sannoh S.E., and Li. X. (2021) A Preliminary Investigation of Coadsorption of Halogens on Engineered Form of Ag0-Aerogel, PNNL-31222, Pacific Northwest National Laboratory, Richland, WA

Nenoff, T. M., Rodriguez M.A., Soelberg N.R., and Chapman K.W. (2014) Silver-Mordenite for Radiologic Gas Capture from Complex Streams: Dual Catalytic CH_3I Decomposition and I Confinement. *Microporous and Mesoporous Materials* 200: 297–303.

Nuclear Regulatory Commission (NRC), 2012, Chapter 10, "Energy: Part 20—Standards for Protection against Radiation," 10 CFR 20. US Nuclear Regulatory Commission, Washington, DC.

Parker G.W. (1964) Release and Transport of UO_2 Fission Products in the Confinement Mockup Facility, Nuclear Safety Program Semiannual Program Report for Period Ending June 31, 1964, ORNL-3 691, p. 3.

Pence, DT, FA Duce, and WJ Maeck. 1972. Developments in the Removal of Airborne Iodine Species with Metal Substituted Zeolites. In Proceedings of Twelfth AEC Air Cleaning Conference (CONF-720823), 417-33 pp. The Harvard Air Cleaning Laboratory, Cambridge, MA.

Pence, DT, FA Duce, and WJ Maeck. 1973. Iodine Adsorbent Program, In Idaho Chemical Programs Annual Technical Report Fiscal Year 1972. Report No. ICP-1022, Idaho National Engineering Laboratory, Idaho Falls, ID.

Scheele R.D., Burger L.L., Matsuzaki C.L. (1983) Methyl iodide sorption by reduced silver mordenite, PNNL 4489

Soelberg, N., Watson, T. (2014) Phase 2 Methyl Iodid Deep-Bed Adsorption Tests, FCRS=SWF-2014-000273, INL/EXT-14-33269

Soelberg, N., Watson, T. (2015) FY-2015 Methyl Iodide Deep-Bed Adsorption Tests Report, FCRD-MRWFD-2015-000267, INL/EXT-15-36817

Soelberg, N, Welty A., and Thomas S. (2018) Initial Results of Iodine Capture from Iodobutane in Vessel Off-gas, NTRD-MRWFD-2018-000189, INL/EXT-18-51574, Idaho National Laboratory

Soelberg N., Welty A.K., Thomas S. (2021) Organic Iodine Capture from Vessel Off-gas, INL/EXT-21-62077, Idaho National Laboratory

Stull D.R. (1947) Vapor Pressure of Pure Substances. Organic and Inorganic Compounds, *Ind. Eng. Chem*., 39, 4, 517-540

Tang S., Choi S., Tavlarides L.L., Shen Z., Wiechert A.I., Yiacoumi S., Ladshaw A., Tsouris C. (2020) Organic Iodides Adsorption Studies on Ag-Aerogel at Various Concentrations and Temperatures (FY20 Updates)

Tavlarides, L.L., Lin, R., Nan, Y., Yiacoumi, S., Tsouris, C., Ladshaw, A., Sharma, K., DePaoli, D. (2015) Sorption Modeling and Verification for Off-Gas Treatment, OE-NFE-12-03822-3

Welty A.K., Soelberg N.R., Bruffey S.H., Greaney A.T. (2021) Updated Engineering Evaluation: Vessel Off-Gas Treatment System for Used Nuclear Fuel Reprocessing Facilities, INL- LTD-21-64587, Idaho National Laboratory

Wilhelm, J.G. and Schuttelkopf H. (1970) Inorganic Adsorber Materials for Trapping of Fission Product Iodine. In Proceedings of the Eleventh AEC Air Cleaning Conference, 568-80 pp. The Harvard Air Cleaning Laboratory, Cambridge, MA.